SIMULATION OF EARTHQUAKE GROUND MOTIONS FOR SAN ONOFRE NUCLEAR GENERATING STATION UNIT 1

SUPPLEMENT II

Submitted to

Southern California Edison Company
2244 Walnut Grove Avenue
Rosemead, California 91770

by

Del Mar Technical Associates
1130 Camino Del Mar, Suite H
Del Mar, California 92014

August 1980

TABLE OF CONTENTS

CHAPTER 1

INTRODUCTION

DELTA's earthquake modeling techniques were developed in order to predict strong ground shaking at specific sites close to earthquake ruptures, where strong motion data are scarce. The modeling procedure has been used to predict the amplitude and character of ground shaking at the San Onofre Nuclear Generating Station in the event of a hypothetical offshore earthquake, eight kilometers from the site. The earthquake model has been described in detail in two reports submitted by Del Mar Technical Associates to Southern California Edison Co., entitled "Simulation of Earthquake Ground Motions for San Onofre Nuclear Generating Station -- Unit 1", Final Report, May 1978, and Supplement 1, July 1979.

The earthquake model has been calibrated against strong motion recordings of the 1940 Imperial Valley earthquake and the 1966 Parkfield earthquake. The results of these studies were presented in the aforementioned reports. The rationale for choosing these particular earthquakes to validate and calibrate the model was the fact that these were large strike-slip earthquakes in Southern California, and the offshore zone of deformation for San Onofre is hypothesized to undergo similar strike-slip motion. These results demonstrated the usefulness of the earthquake model for predicting peak values of acceleration, velocity and displacement and for obtaining suitable estimates of strong motion response spectra.

Further validation of DELTA's earthquake model has been performed against strong motion data recorded during the 1933 Long Beach and 1971 San Fernando earthquakes. The results of these studies are contained in the following report. The Long Beach earthquake was a strike-slip coastal earthquake with an estimated magnitude of $M_L \simeq 6.3$. It yielded strong motion recordings at three nearby stations. The 1971 San Fernando earthquake ($M_L \simeq 6.4$) was a thrust event. The strong motion data recorded at Pacoima Dam have been modeled to test the usefulness of the earthquake model for simulating the large accelerations recorded at that station.

Modifications have been introduced into DELTA's earthquake model since Supplement 1 of July 1979. The dip orientation of each 1-km-square segment of rupture surface has been randomized so that it deviates from the gross dip of the fault plane by a random number with a two-thirds confidence of not exceeding 10 degrees. The orientation of the rake of the slip vector in each rupture segment has been modified by a random number with a two-thirds confidence of not exceeding 20 degrees. The dip and rake incoherence were introduced in order to describe the uncertainty in our knowledge of the rake and dip of the rupture surface on a scale much smaller than the overall dimensions of the earthquake fault. These extensions to the earthquake model augment the randomness in the 1-km-square cell strike orientation, the rupture direction, and the orientation of the particle motions at the receiver as described in Supplement 1 of July 1979.

CHAPTER 2

MODELING THE 1933 LONG BEACH EARTHQUAKE

2.1 OVERVIEW

The 1933 Long Beach earthquake occurred along the coastline of Southern California, causing loss of life and widespread property damage in the adjoining coastal communities. This section is concerned with modeling the strong ground motions recorded during the 1933 Long Beach event, in order to examine the applicability of DELTA's earthquake model for prescribing ground motions for Southern California coastal earthquakes.

There is considerable uncertainty associated with our knowledge of the fault parameters for the Long Beach earthquake. Due to the sparsity of regional seismograph stations in 1933 and the complex geologic structure in this area, the epicentral location is poorly constrained. Two estimates for the epicenter are 33°37'N, 117°58'W (Trifunac and Brady, 1975) and 33°35'N, 117°59°W (Blume, 1977). Since there is no evidence of surface breakage for this event, the precise location and extent of faulting are not known. Nevertheless, estimates for the various fault parameters can be made. Depth of faulting may be inferred from the depth of the seismically active crust, which is generally taken to be somewhat less than 15 km in this region. Distribution of aftershocks and property damage indicate that the rupture extended in a northwest direction from the epicenter, thus placing the deformation along the Newport-Inglewood fault zone. The aftershocks extended approximately 45 km from the epicentral area (Woodward Clyde Consultants, 1979), which gives some indication of the length of rupture.

The focal mechanism for the Long Beach earthquake has been estimated in a study which models the waveforms of seismograms recorded at regional and teleseismic distances (Woodward Clyde Consultants, 1979). The results of this study indicate a dip of 80°N to 100°N, a strike of

N40°W to N45°W, a hypocentral depth of 9 to 12 km, a moment of 6.2×10^{25} dyne-cm and a relative block motion which is predominantly strike-slip for this event.

Three strong motion recordings were obtained during the Long Beach earthquake: at the subway terminal in Los Angeles (SBWY), at the Central Manufacturing District Terminal in Vernon (VERN) and at the Public Utilities Building in Long Beach (LNGB). These were the first strong motion accelerograms ever recorded. Due to a variety of reasons, these data are less than ideal. According to Blume (1977), the accuracy of the spectral components for periods greater than about two seconds is doubtful, due to inadequate instrument amplification. Both the SBWY and VERN instruments triggered late. An additional factor which affected the data at SBWY is the fact that the accelerograph was situated 19.5 meters beneath the ground surface. Possible effects of instrument burial on the recorded data at this station are investigated in Section 2-4.

The geologic structure in the area of the Long Beach earthquake and the recording stations is rather complicated. The Los Angeles basin is situated immediately northeast of the Newport-Inglewood fault. The depth to the basement complex varies considerably in the region of the fault and the recording stations. Overlying the basement complex is a thick unit of soft sediments, which exhibits a contrasting velocity profile beneath each of the recording stations. The earth model chosen to represent the regional geology in this study represents a compromise between the geologic sections beneath each of the recording stations and in the fault zone as provided by URS/John A. Blume & Associates, Engineers (1978). The geologic model consists of ten horizontal visco-elastic layers overlying a viscoelastic semi-infinite half-space with the individual layer properties listed in Table 2-1.

TABLE 2-1

Viscoelastic Parameters for the Long Beach Earth Structure

Depth to Top of Layer (km)	Layer Thickness (km)	P-Wave Velocity (km/sec)	S-Wave Velocity (km/sec)	ρ Density (g/cc)	Q_p Compressional Quality Factor	Q_s Shear Quality Factor
0.	.015	.85	.45	1.9	30	15
.015	.2	1.	.55	2.1	35	15
.215	.4	1.5	.8	2.15	60	23
.615	.25	1.9	1.	2.2	81	30
.865	.15	2.3	1.2	2.25	104	38
1.105	.6	2.7	1.5	2.35	121	50
1.615	.5	3.1	1.7	2.5	145	58
2.115	.3	3.4	1.9	2.55	161	67
2.415	.6	3.9	2.2	2.6	189	80
3.015	.3	4.5	2.5	2.6	229	94
3.315	∞	6.1	3.4	2.7	334	139

2.2 RESULTS

Since the fault geometry of the Long Beach earthquake is not well constrained, much of the effort in this study has been devoted to determining a set of source parameters that provide an optimal fit between the response spectra for the observed data and for the ground motions computed using DELTA's earthquake model. In this section, the parameters defining the preferred earthquake model are presented, along with the fit to the response spectra for the observed data. In addition, the observed accelerograms are compared with a set of acceleration time-histories computed using the preferred fault model.

The parameters of the Long Beach fault model which provide an optimal fit to the response spectra for the recorded ground motions are presented in Table 2-2. A plan view of the fault trace for the preferred earthquake model is shown as a solid line in Figure 2-1. The rupture surface consists of a single fault plane, 40 km long and 12 km wide. The depth to the top of the rupture surface is 0.5 km. The fault plane has a strike of N39°W, a dip of 90° and a relative block motion which is predominantly strike-slip. The slip function remains constant over the fault surface. The initial slip velocity is 800 cm/sec and the rise time is 4.4 sec as given by the fault width divided by the shear wave velocity. The fault offset is 140 cm.

The fit to the response spectra for the observed data is shown in Figures 2-2, 2-3 and 2-4. The top diagrams show the vertical components and the bottom diagrams show the horizontal components for each receiver. In order to illustrate the effects of using different random number sequences in DELTA's earthquake model, the calculated response spectra of the computed ground motions are presented in terms of the mean (solid curves) and the mean plus and minus one standard deviation (long and short dashed lines) at each period for the response spectra of seven individual ground motion simulations computed using seven independent random number sequences. The short dashed lines represent the response spectra calculated from the observed ground motion. All the curves correspond to

TABLE 2-2

PARAMETERS FOR PREFERRED MODEL OF THE LONG BEACH EARTHQUAKE

FAULT PARAMETERS

Fault Length (km)	Fault Width (km)	Shallowest Extent (km)	Hypocenter Depth (km)	Fault Strike	Fault Dip	Slip Direction
40.	12.	.5	12.5	N39°W	90°	-15°*

SLIP FUNCTION PARAMETERS

Initial Slip Velocity (cm/sec)	Slip Duration (sec)	Fault Offset (cm)
800	4.4	140

SEISMIC MOMENT

1.7×10^{26} dyne-cm

*Predominantly right lateral strike-slip faulting. West block moves upwards relative to east block.

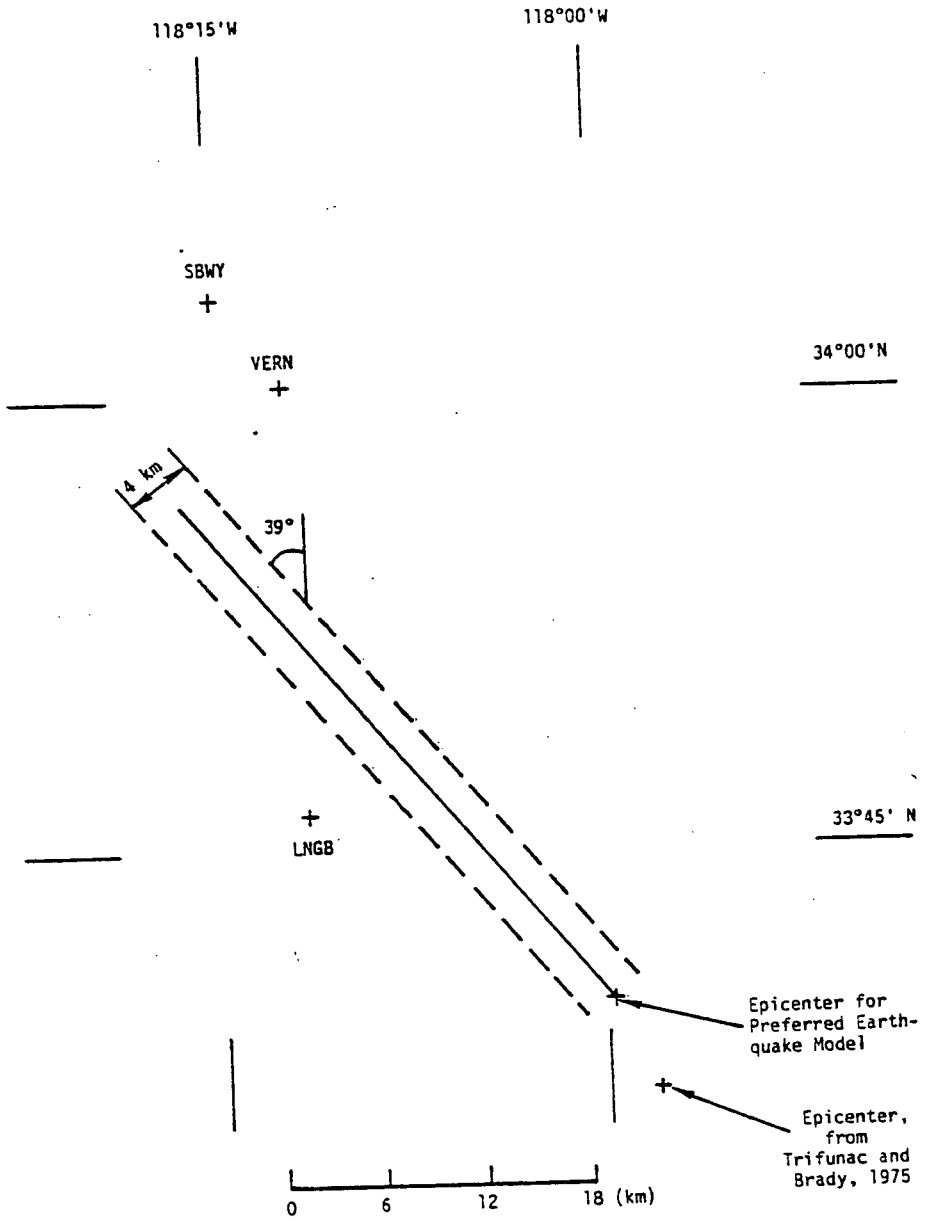

Figure 2-1. Map of the preferred fault model for the 1933 Long Beach Earthquake (solid line). The dashed lines represent fault traces for two alternate earthquake models investigated in this study.

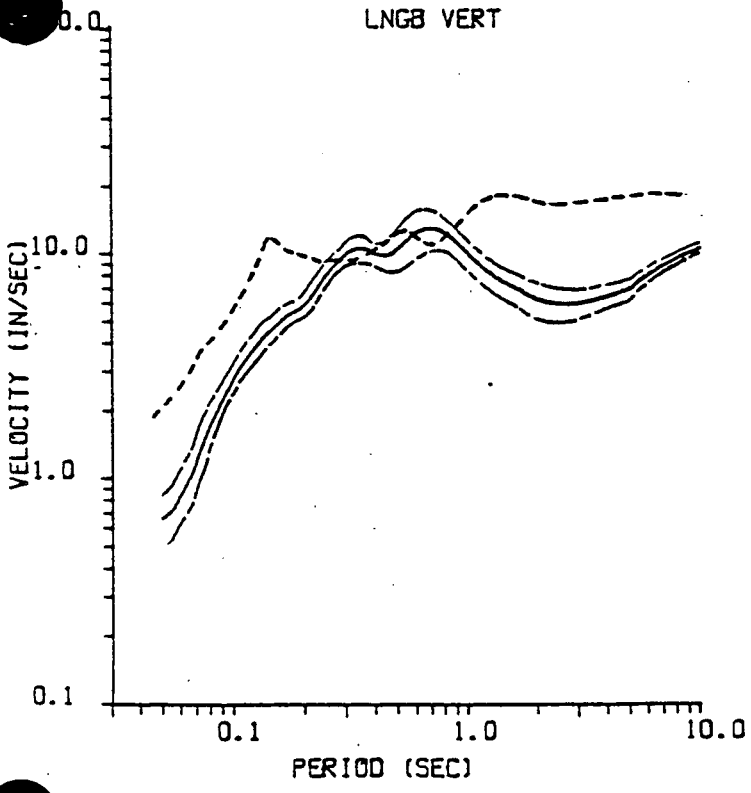

Figure 2-2. Comparison of the smoothed 2% velocity response spectra observed at Station LNGB and computed from the preferred model of the Long Beach Earthquake.

- - - - — Observed

——— Calculated Mean

——·—— Calculated Mean ± 1 Standard Deviation

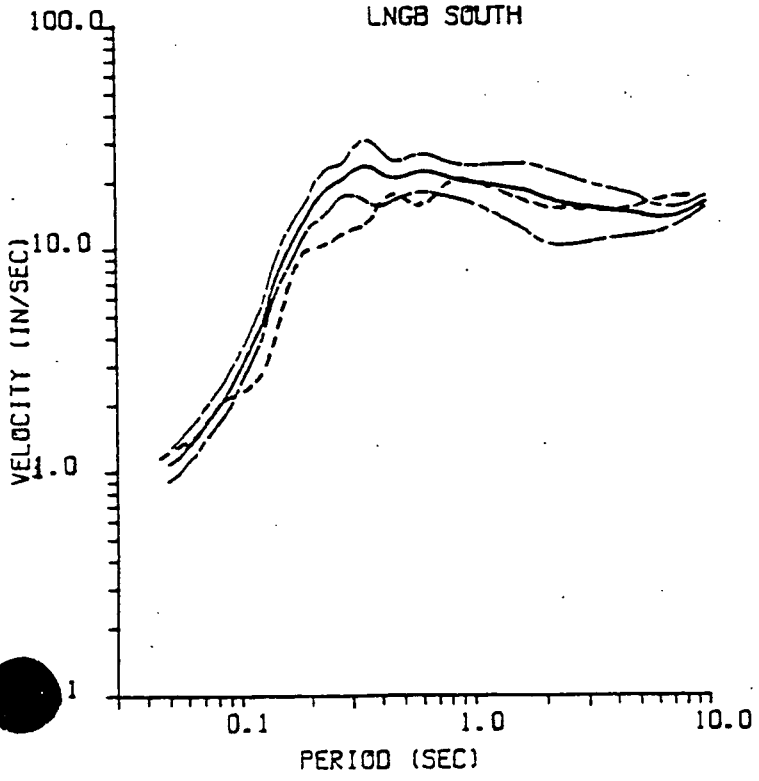

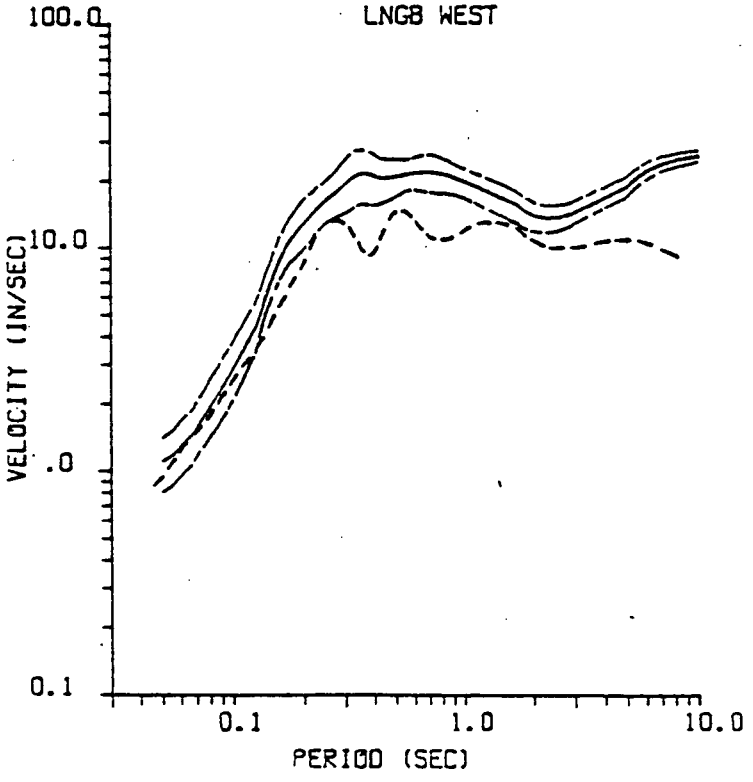

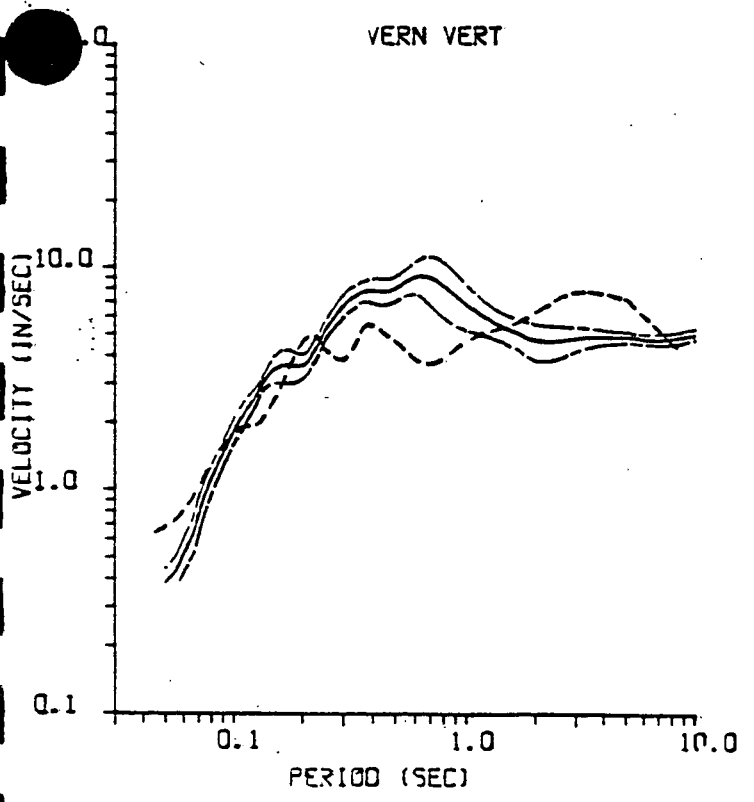

Figure 2-3. Comparison of the smoothed 2% velocity response spectra observed at Station VERN and computed from the preferred model of the Long Beach Earthquake.

- Observed
- Calculated Mean
- Calculated Mean ± 1 Standard Deviation

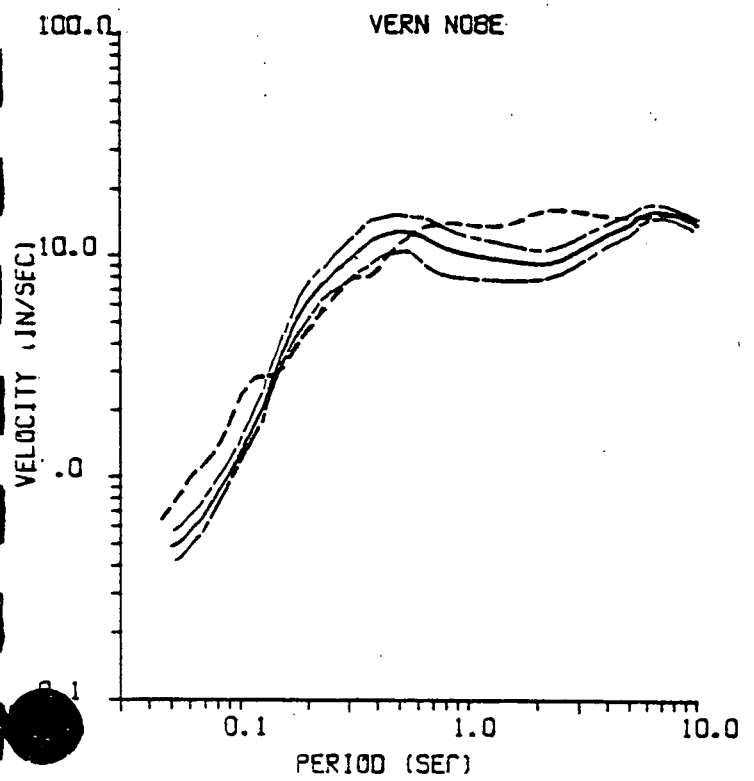

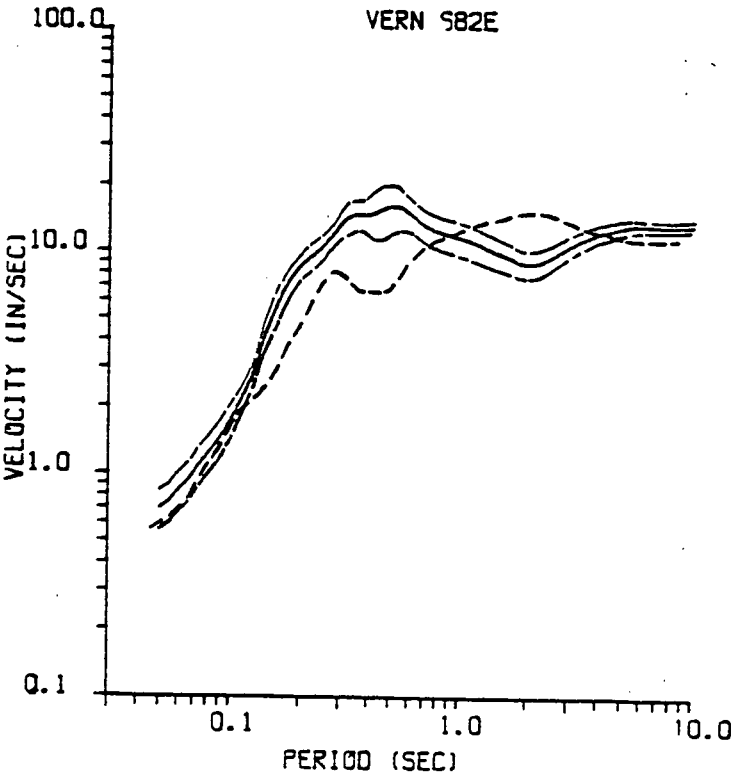

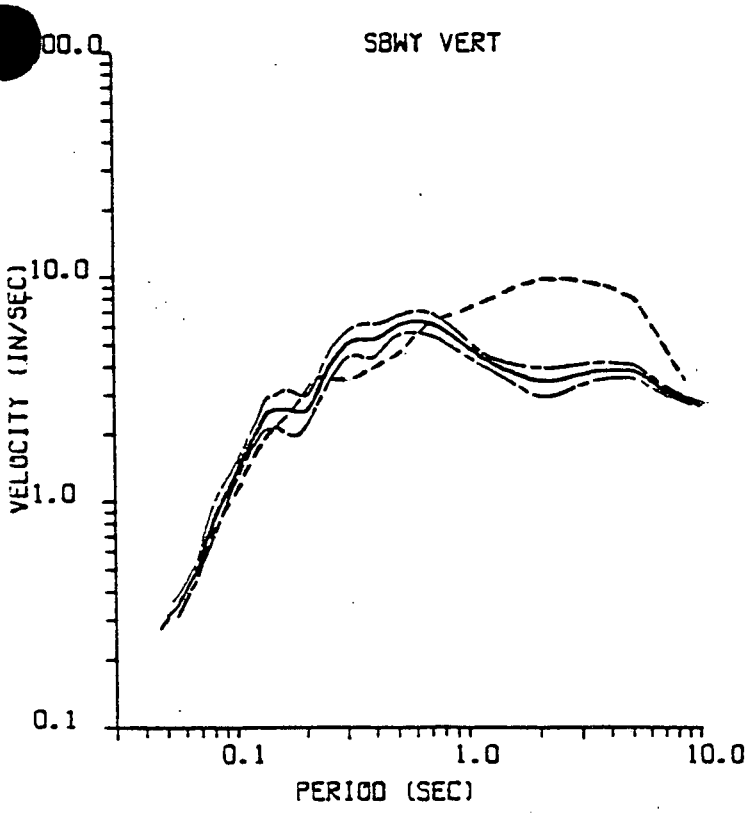

Figure 2-4. Comparison of the smoothed 2% velocity response spectra observed at Station SBWY and computed from the preferred model of the Long Beach Earthquake.

- Observed
- Calculated Mean
- Calculated Mean ± 1 Standard Deviation

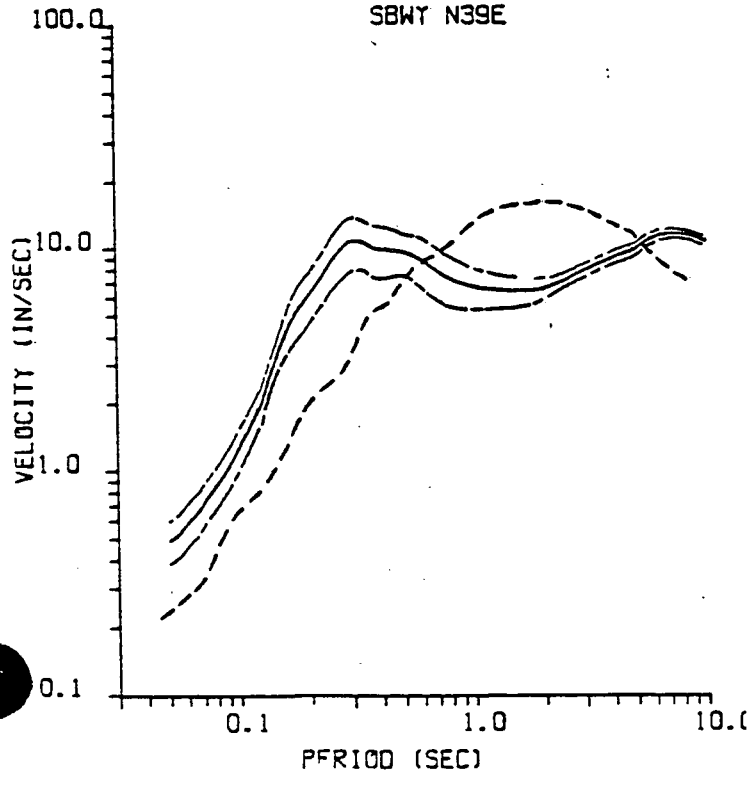

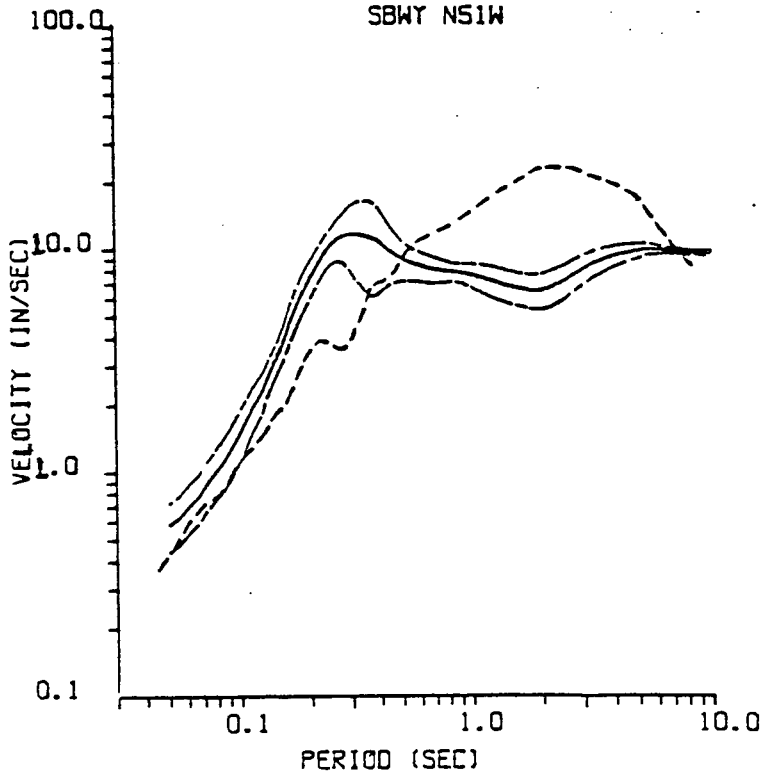

the smoothed, 2% damped response spectra. The agreement between the observed and computed response spectra is very good. Of all the calculated horizontal components, only VERN N08E is deficient at high frequencies. The high frequency computed response spectra for SBWY are somewhat higher than the observed values for the horizontal components. However, when the effects of station burial are taken into account (see Section 2-4), the fit is actually quite good. The computed vertical response spectrum for Station LNGB is deficient at high frequencies. It should be pointed out that the calculated vertical high frequency ground motion is substantially larger than the high frequency horizontal ground motions recorded at this station.

The maximum acceleration, velocity and displacement values for the computed ground motions are compared to the corresponding observed values in Table 2-3. Except for the vertical component at Station LNGB, and to a lesser degree the vertical component for VERN, the peak accelerations for the computed ground motions are conservative relative to the observed values. In particular, the mean of the maximum computed horizontal accelerations for VERN N08E is larger than the observed peak value in spite of the fact that the computed high frequency response spectral values are lower.

Table 2-3 shows that, with a few exceptions, the calculated peak velocity and displacement values agree well with the observed values. Similar agreement is obtained for the response spectra comparisons at intermediate and long periods. The largest discrepancies occur for the VERT and SOUTH components at Station LNGB in Figure 2-2. Also, the shapes of the computed and observed intermediate and long period response spectra for Station SBWY are somewhat different, as shown in Figure 2-4. This discrepancy is not related to the effects of instrument burial, as discussed in Section 2-4, since the intermediate and long period data are not influenced by subsurface burial at Station SBWY. Minimal effort was investigated into matching the intermediate and long period response spectra for station SBWY since, as was pointed out in Section 2-1, the accuracy of these data is questionable.

TABLE 2-3

Maximum Values of Acceleration, Velocity and Displacement for Long Beach Earthquake

Station	Component	Acceleration (g) Obs.	Acceleration (g) Calc.*	Velocity (cm/sec) Obs.	Velocity (cm/sec) Calc.*	Displacement (cm) Obs.	Displacement (cm) Calc.*
LNGB	Vertical	.29	.18 (.05)	30	13 (.8)	26	21 (1.4)
	South	.20	.35 (.06)	29	32 (8.7)	23	34 (2.4)
	West	.16	.35 (.10)	16	43 (5.1)	12	46 (2.4)
VERN	Vertical	.15	.1 (.01)	12	9 (.8)	7	13 (.4)
	N08E	.13	.15 (.03)	29	28 (4.)	15	20 (1.5)
	S82E	.15	.22 (.05)	17	21 (2.6)	18	25 (1.5)
SBWY	Vertical	.06	.09 (.02)	9	6 (1.0)	6	8 (.5)
	N39E	.06	.16 (.03)	17	17 (1.4)	8	16 (1.3)
	N51W	.10	.19 (.05)	24	15 (2.9)	16	15 (1.9)

*Mean values for seven simulated recordings. One standard deviation shown in brackets.

In Figures 2-5, 2-6 and 2-7, the observed and computed acceleration time histories are compared for Stations LNGB, VERN and SBWY, respectively. Each seismogram is self-scaled to its respective absolute maximum peak and the scaling factors are displayed above each time history. The computed accelerograms correspond to a single representative set of time histories chosen from the series of seven ground motion recordings computed using independent random number sequences. The reference times ($t = 0$) for the observed accelerograms correspond to the instant that the ground shaking was strong enough to trigger each of the recording instruments. The reference times for the computed records correspond to the instant that rupture initiated at the hypocenter in the earthquake simulation model. Therefore, the calculated seismograms appear delayed relative to the observed seismograms. Due to the idealistic earth structure and rupture physics used in DELTA's earthquake model, the duration of shaking is shorter for the computed accelerograms. Although the output of the earthquake ground motion computations is a set of three component seismograms, it was not the objective of this study to obtain "wiggle-for-wiggle" fits to the recorded data. Such an undertaking would probably entail inversion for a more complex rupture sequence as well as a more refined geologic model, which is beyond the scope of this study. Instead, the objective here was to reproduce the important features of the recorded ground motion through response spectral fitting, using fairly simple rupture models.

The suite of seven acceleration time histories calculated for Station LNGB using the seven independent random number sequences is shown in Figures 2-8 through 2-10 for the three components of ground motion. The overall features of the seismograms for each component are basically independent of the particular random number sequence used, although the peak acceleration values show some variations (refer to Table 2-3 for the one standard deviation values in peak acceleration for each component.

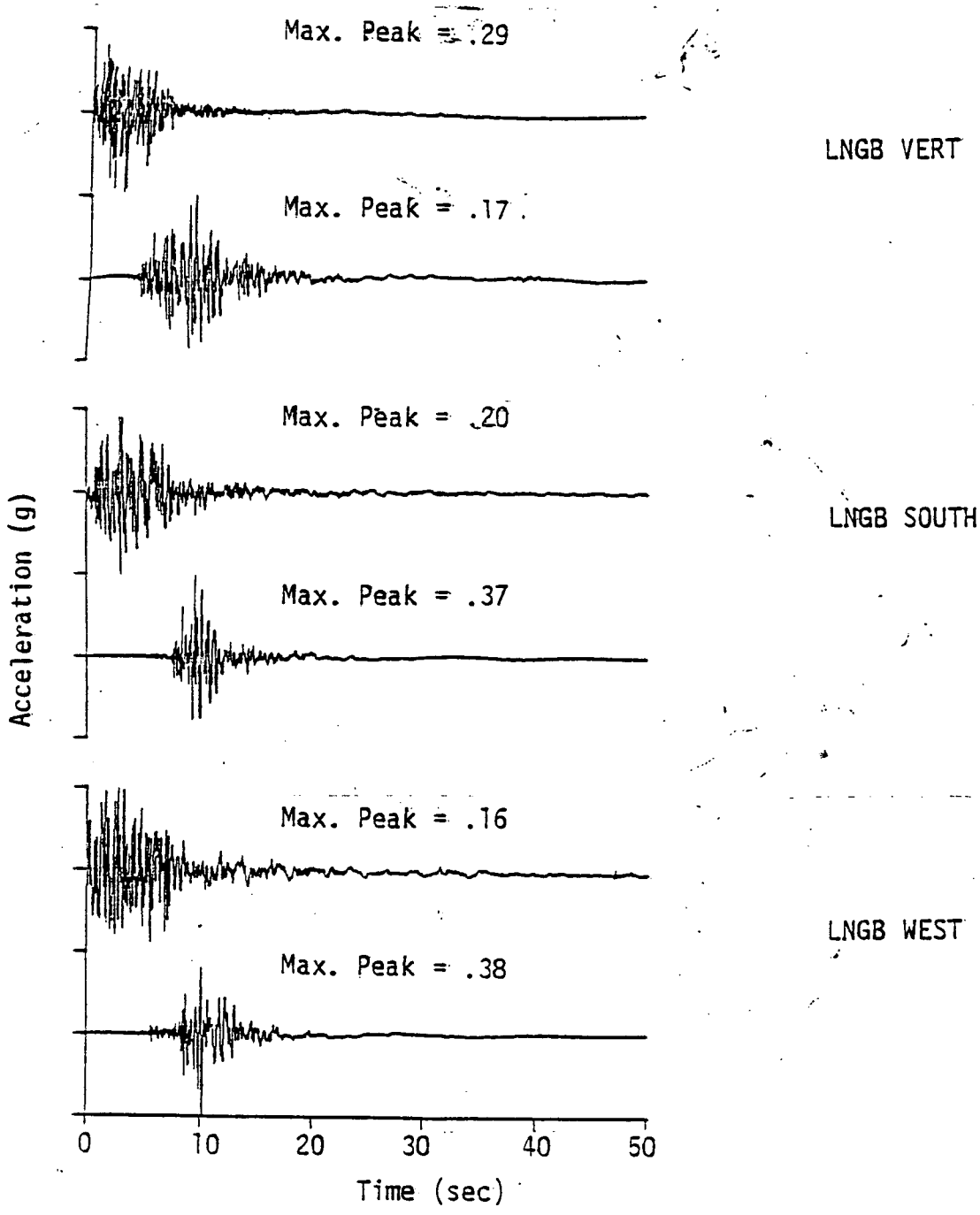

Figure 2-5. Comparison of the three components of acceleration observed at station LNGB (above) and computed from the preferred model of the Long Beach Earthquake (below).

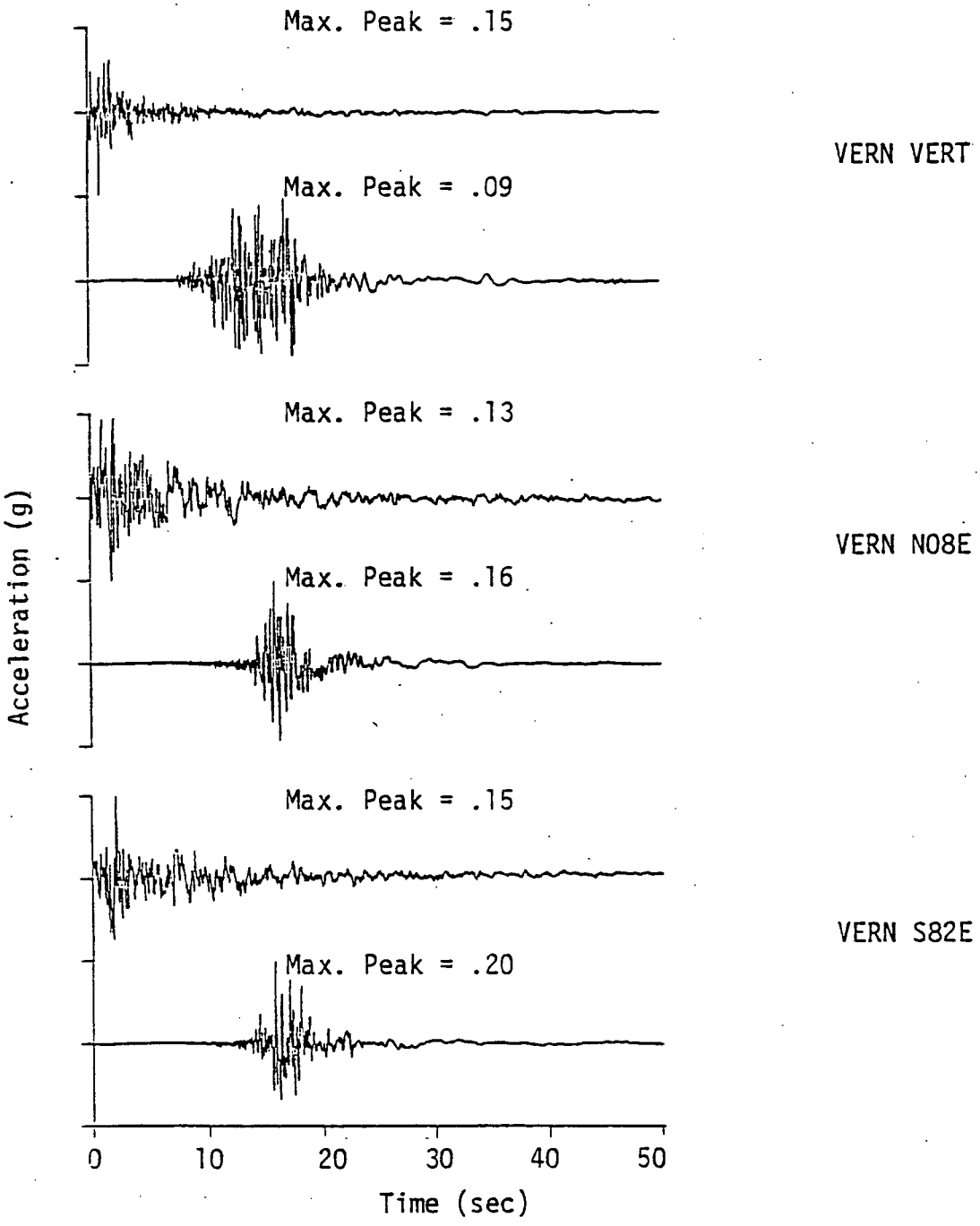

Figure 2-6. Comparison of the three components of acceleration observed at station VERN (above) and computed from the preferred model of the Long Beach Earthquake (below).

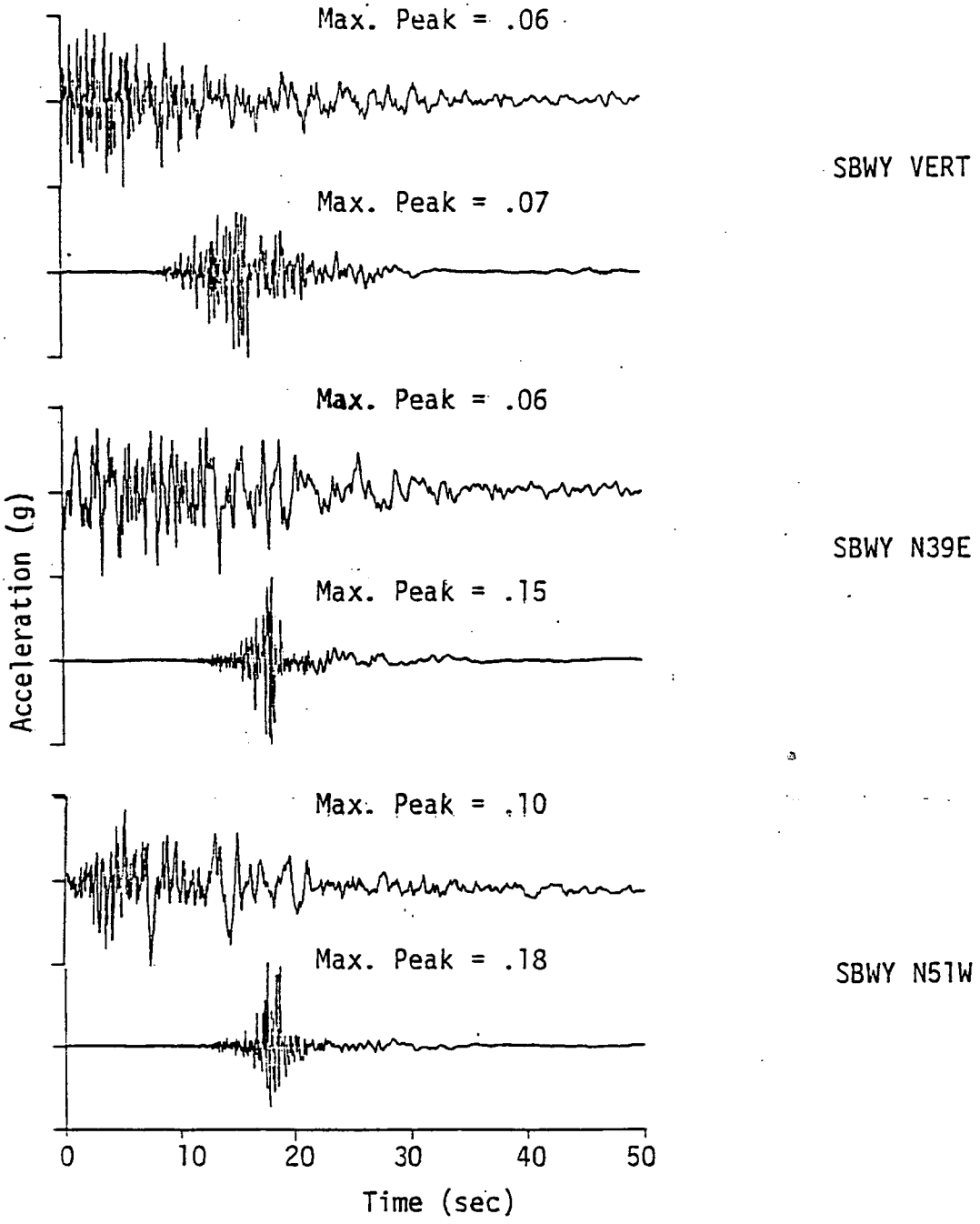

Figure 2-7. Comparison of the three components of acceleration observed at station SBWY (above) and computed from the preferred model of the Long Beach Earthquake (below).

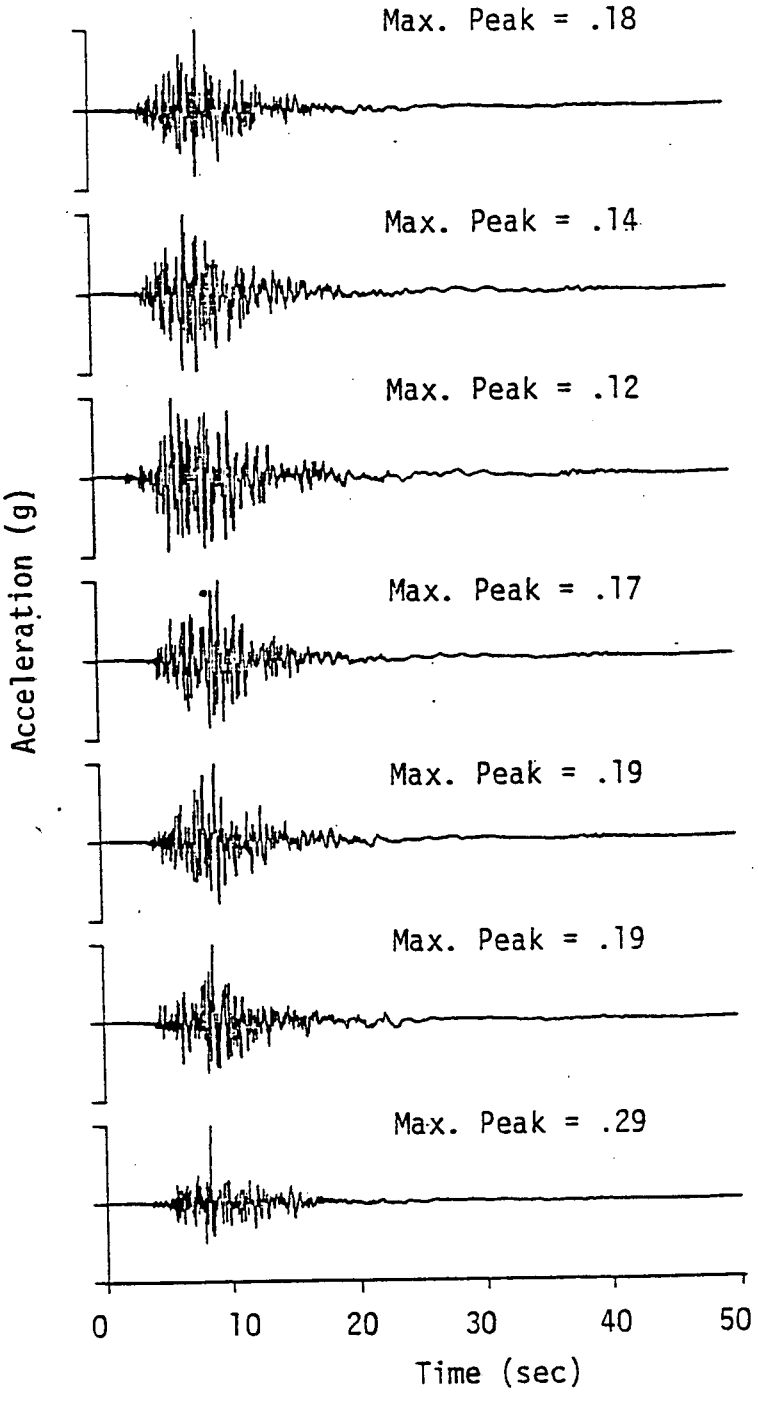

Figure 2-8. Comparison of the acceleration time histories computed for LNGB VERT using seven independent random number sequences in the preferred earthquake model.

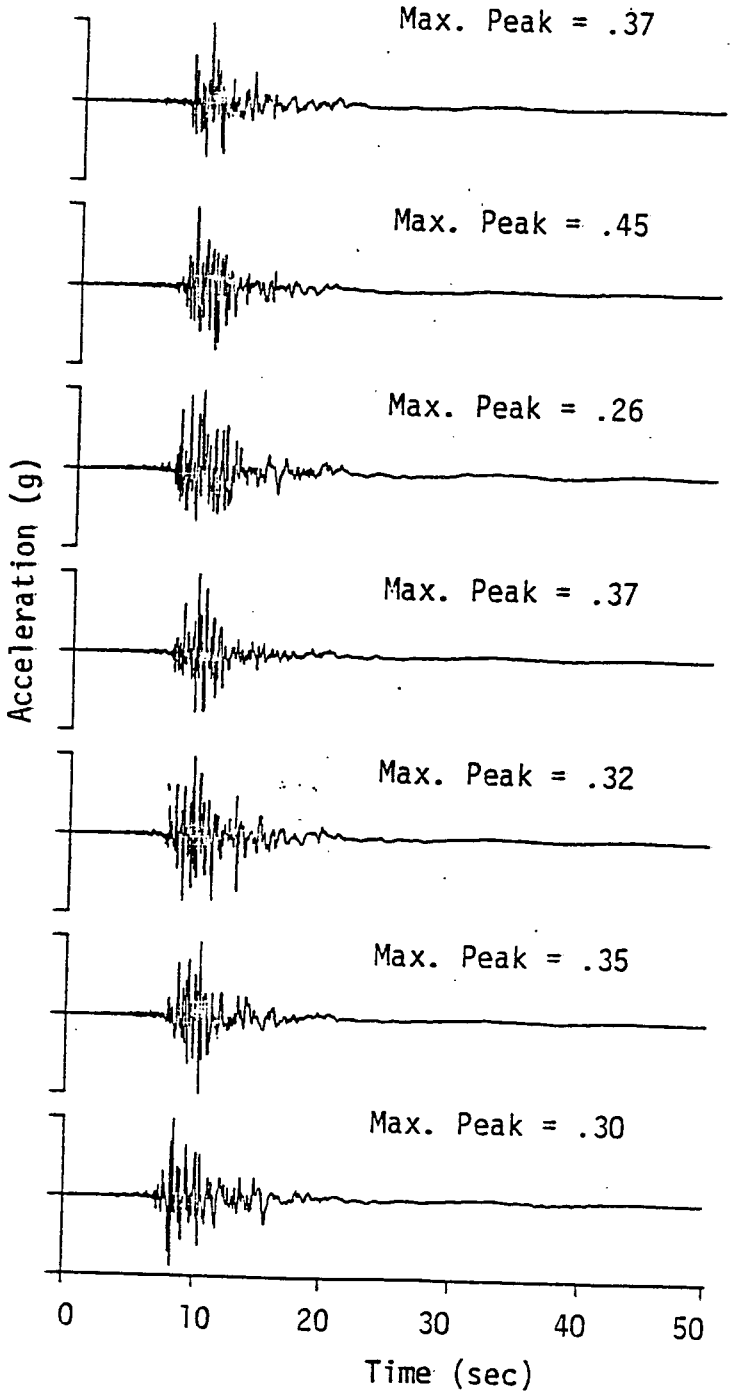

Figure 2-9. Comparison of the acceleration time histories computed for LNGB SOUTH using seven independent random number sequences in the preferred earthquake model.

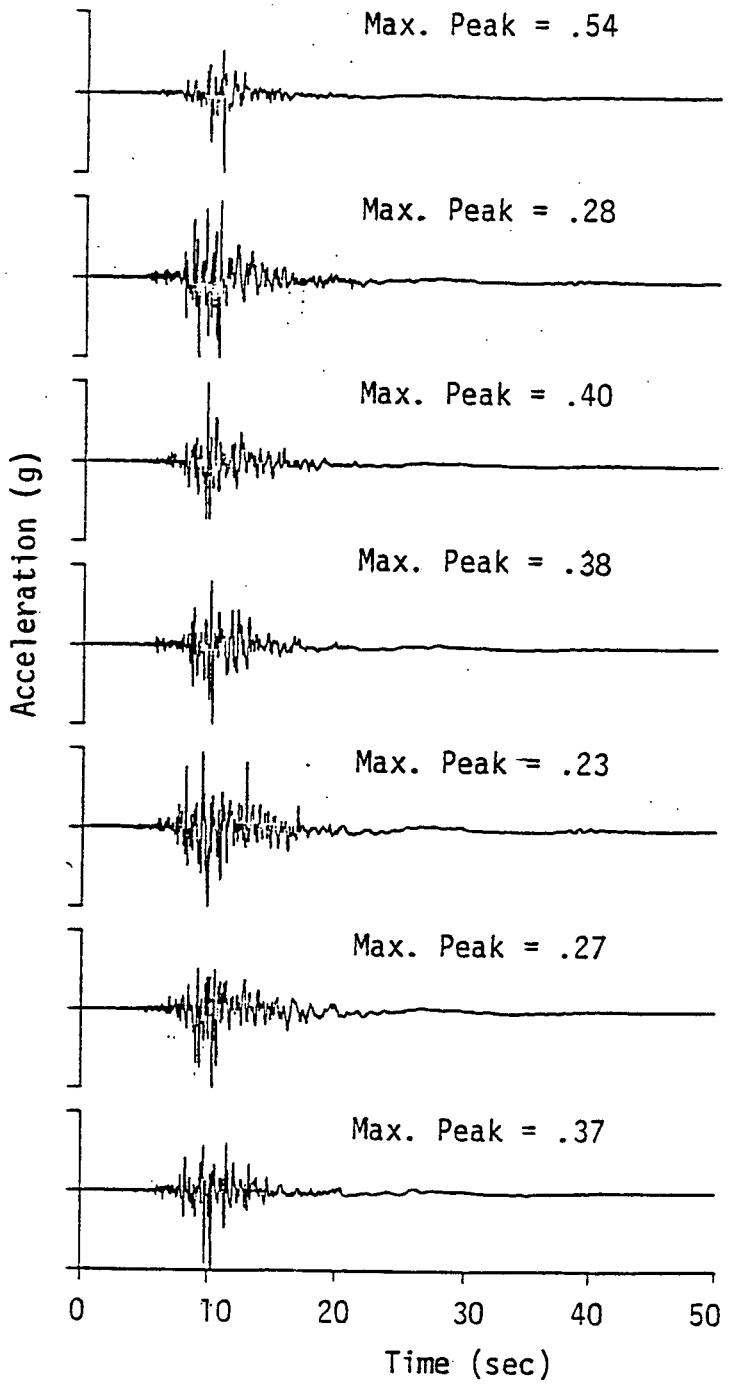

Figure 2-10. Comparison of the acceleration time histories computed for LNGB WEST using seven independent random number sequences in the preferred earthquake model.

2.3 DISCUSSION OF RESULTS

In the previous section, a fault model was investigated which gave an optimal fit to the response spectra for the ground motions recorded during the Long Beach Earthquake. In this section, the source parameters for the preferred earthquake model are compared with the source parameters for the Long Beach earthquake as deduced in other studies. In general, the fault parameters for the various studies were found to be highly consistent. The sensitivity of the response spectra for the computed ground motions to changes in various fault parameters for the preferred earthquake model is also investigated in this section.

The aftershock zone for the Long Beach earthquake was about 45 km in length. The fault lengh for the preferred earthquake model is 40 km. The fit to the data at Stations SBWY and VERN constrains the northwest end of the rupture surface (see Figure 2-1) for the preferred earthquake model. If the rupture plane is shortened at the northwest end, the response spectra for the computed ground motions at SBWY and VERN are deficient relative to the observed spectra. The southeast end of the rupture surface is controlled by the epicenter location. Various researchers have placed the epicenter further south and east of the epicentral location as used in the preferred earthquake model. However, calculations using the preferred Long Beach earthquake model but with the fault length altered by as much as 5 km at the southeast end have negligible influence on the computed response spectra. Therefore, the fault length could be increased in the southeast direction, allowing the total fault length for the preferred earthquake model to approach the length of the aftershock zone without affecting the fit to the data.

The strike of the rupture surface for the preferred model of the Long Beach Earthquake is N39°W. This is consistent with the strike of the aftershock sequence, N35°W to N45°W and with the strike for this event as deduced in a focal mechanism study, N40°W to N45°W (Woodward-Clyde Consultants, 1979). The dip angle and slip direction for the preferred fault model are also consistent with the corresponding estimates

determined in the same focal mechanism study. In the course of this study it was found that the response spectra for the computed ground motions were insensitive to small changes in the slip direction.

The shortest distance between Station LNGB and the surface trace of the fault in the preferred model for the Long Beach earthquake is about 6 km, which is comparable to estimates for the shortest distance between Station LNGB and the surface trace of the Newport-Inglewood Fault (4.5 to 5.0 km). The effects of changing the location of the rupture surface for the preferred earthquake model in such a way that the surface trace of the fault is 2 km closer to and 2 km further from Station LNGB are investigated in Figure 2-11. The surface traces for these alternate fault models are shown as dashed lines in Figure 2-11. In each case, the rupture surface is displaced 2 km in a direction perpendicular to the fault strike; all other parameters for these fault models are identical to those for the preferred earthquake model.

The solid curves in Figure 2-11 represent the mean for the smoothed 2% damping response spectra for seven independent ground motions computed from the preferred Long Beach earthquake model. The dashed curves represent the mean for the smoothed 2% damping response spectra for four independent ground motions computed from the alternate fault models. The results indicate that the response spectra for all periods are shifted either upwards or downwards relative to the response spectra for the preferred earthquake model, depending on whether the closest distance from the station to the surface trace of the fault is decreased or increased, respectively.

There is no evidence of any surface breakage for the 1933 Long Beach earthquake and it is difficult to estimate the depth to the rupture surface for this event. The effects of changing the depth to the top of the fault surface for the model of the Long Beach earthquake are shown in Figure 2-12. The solid curve represents the mean response spectra for ground motions computed using seven random number sequences in the preferred model. The short dashed lines and long dashed lines represent the mean response spectra for ground motions computed using four random

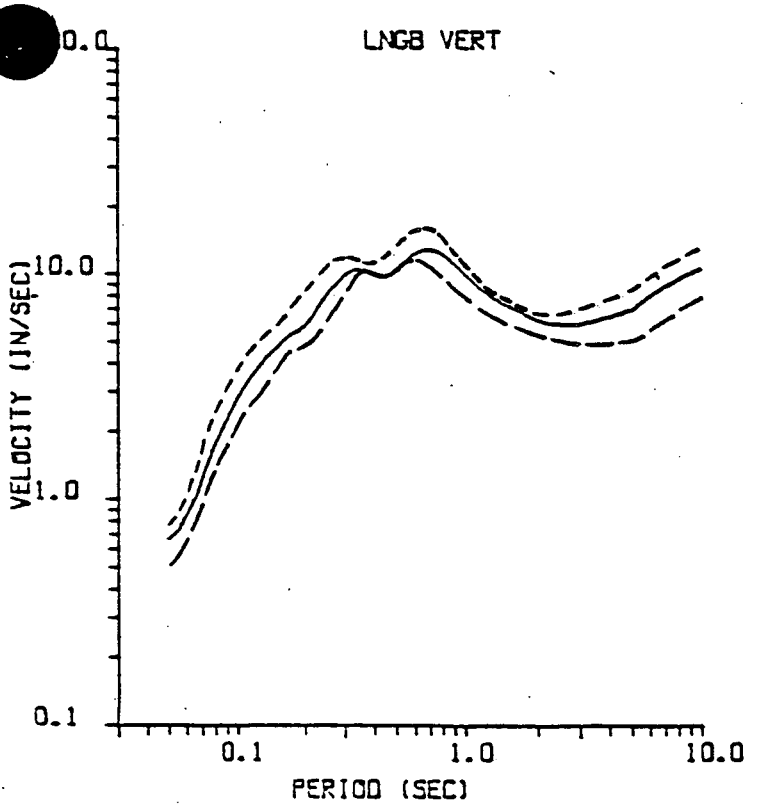

Figure 2-11. Comparison of the smoothed 2% velocity response spectra computed from three earthquake models at different distances from station LNGB. Surface traces for these faults are shown in Figure 2-4.

Mean for Preferred Fault Model

Mean for Fault 2 km Further From LNGB

Mean for Fault 2 km Closer to LNGB

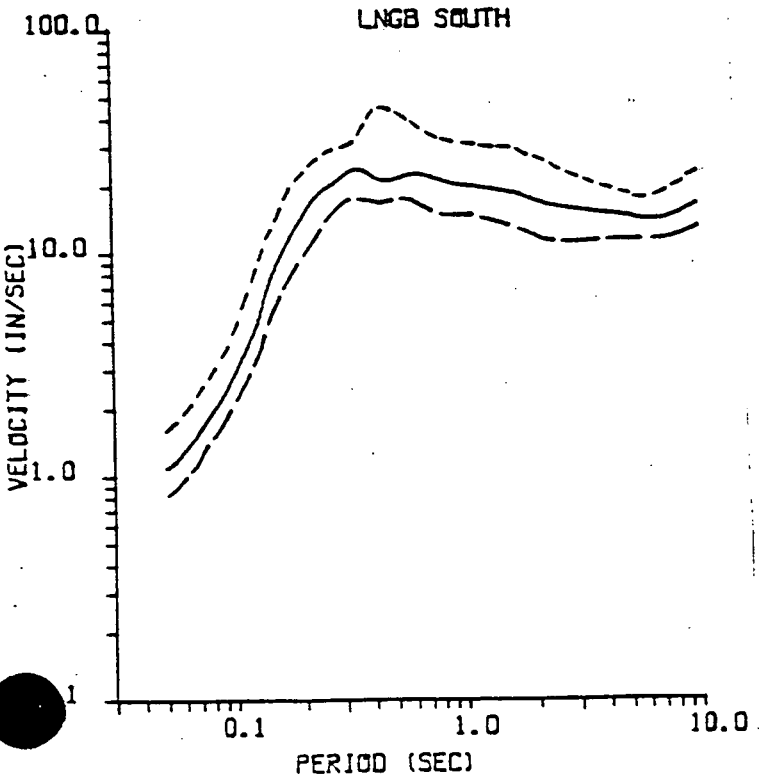

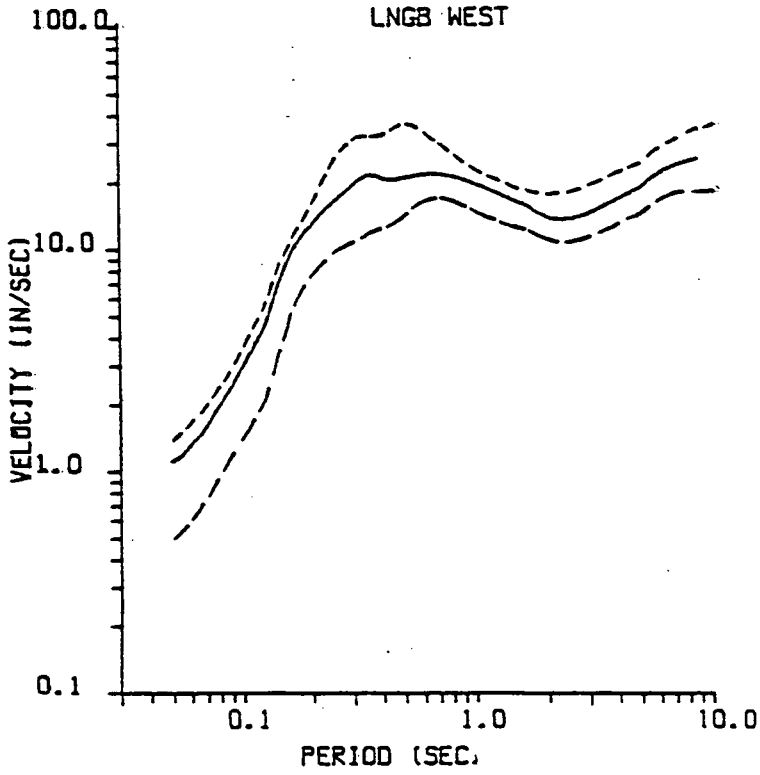

number sequences in alternate models with fault tops at depths of 1.5 and 2.5 km, respectively. Except for the depth to the rupture surface and the rise time, all the other source parameters in the alternate models are identicaly to those for the preferred earthquake model. The rise time is determined by the fault width divided by the shear wave velocity, leading to rise times of 4.4, 3.6 and 3.0 seconds for the three fault models with fault tops at 0.5, 1.5, and 2.5 km, respectively. The response spectra in Figure 2-12 indicate that a negligible amount of energy is radiated from the rupture in the top few kilometers of sediments. This phenomenon can be attributed to the low rigidity of the surficial layers (see Table 2-1). It should be pointed out in these sensitivity studies that small discrepancies (well within one standard deviation) could arise due to necessarily using slightly different random sequences between the different models.

The depth of the seismically active crust in the region of the Long Beach earthquake is generally accepted to be less than about 15 km. The depth of the fault bottom for the preferred model of the Long Beach earthquake is 12.5 km. The effects of varying the depth of the fault bottom are shown in Figure 2-13. The solid curves represent the mean response spectra for the preferred earthquake model. The short dashed curves and long dashed curves represent the mean response spectra for four independent random rupture sequences computed from models with fault bottoms at 10 and 15 km respectively. The corresponding rise times used in these alternative earthquakes are 3.7 seconds and 5.1 seconds. Only the fault bottom depths and rise times for these alternate models have been changed; all the other source parameters are identical to those used in the preferred earthquake model. In general, using a deeper fault bottom in the earthquake model leads to a somewhat higher response spectrum. However, the response spectra for Station LNGB shown in Figure 2-13 seem to be rather insensitive to small changes in the fault bottom depth.

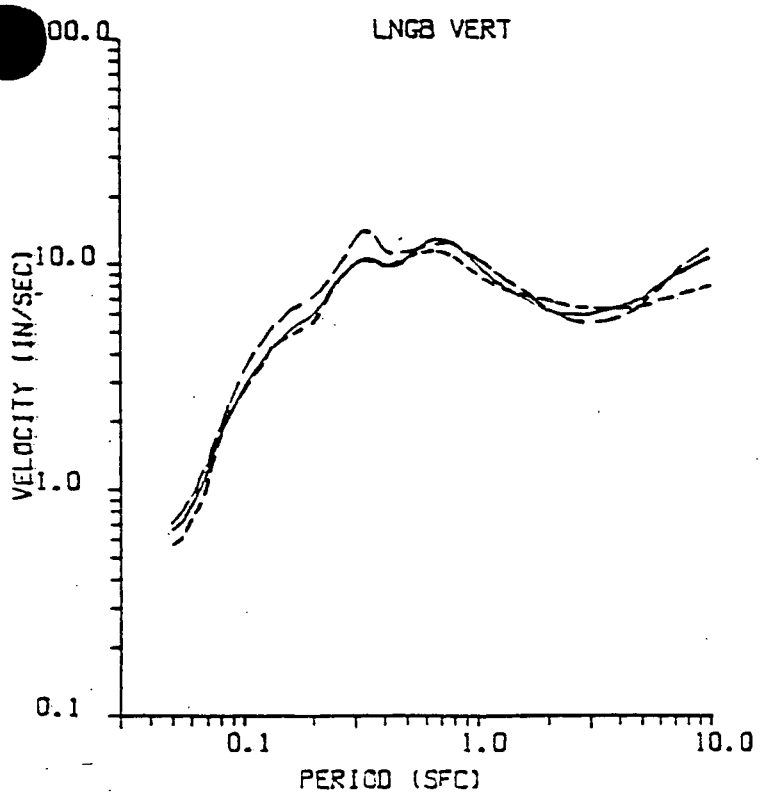

Figure 2-13. Comparison of the smoothed 2% velocity response spectra computed from three earthquake models with fault bottoms at different depths.

——— Mean, Fault Bottom at -12.5 km (Preferred Fault Model)

– – – – – Mean, Fault Bottom at -10 km

— — — Mean, Fault Bottom at -15 km

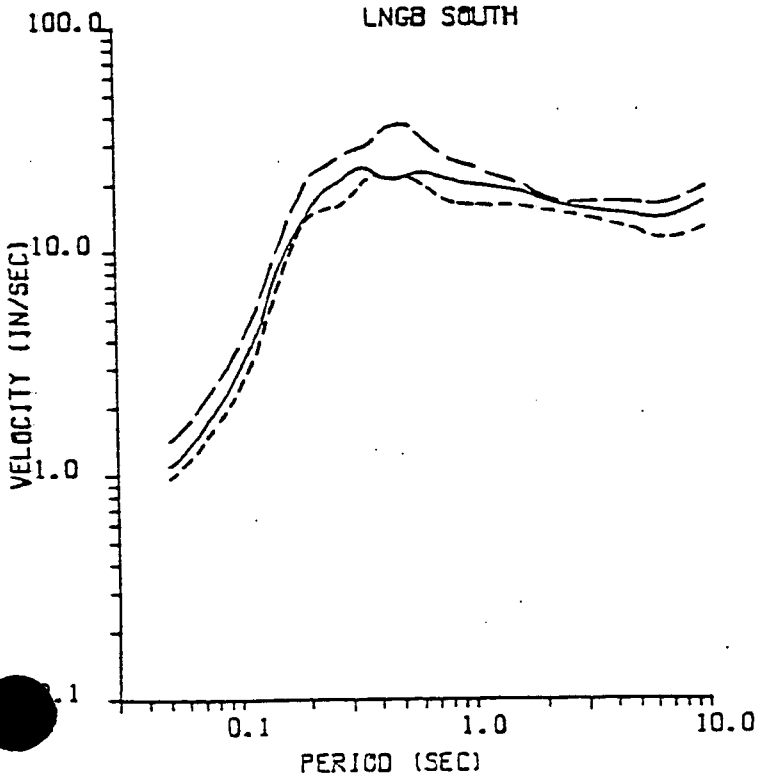

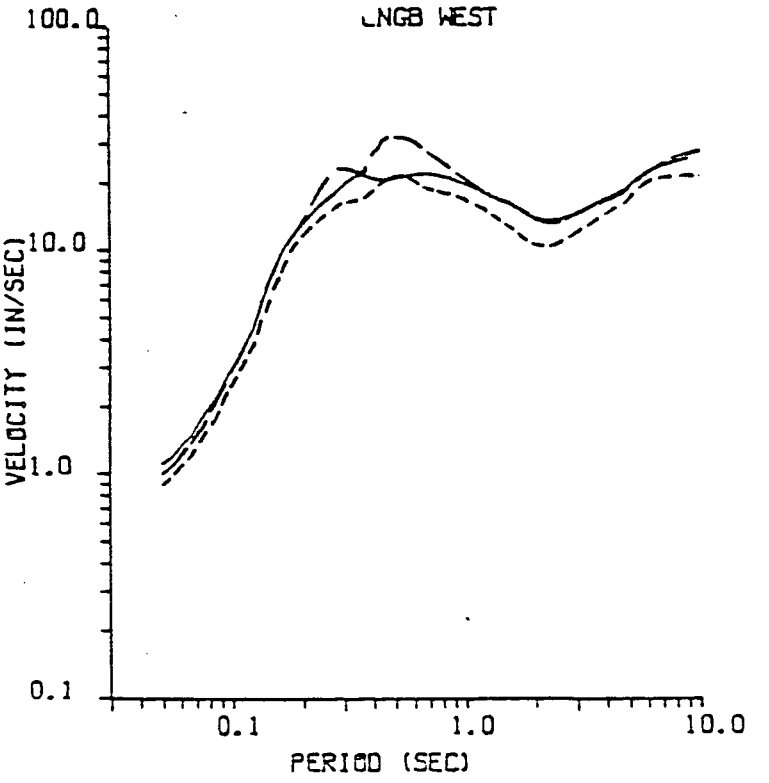

The seismic moment of an earthquake is calculated from

$$\text{Seismic Moment} = M_o = \sum_{i=1}^{N} \mu_i A_i \delta_i$$

in which the summation extends over the layers containing the fault; μ_i, A_i, and δ_i are the shear modulus, area of the fault and slip amplitude (fault offset), respectively, in the i^{th} layer. Using this formula, the seismic moment for the preferred model of the Long Beach earthquake is calculated to be 1.7×10^{26} dyne-cm. In comparison, a study which involved modeling six regional and teleseismic recordings of the 1933 Long Beach earthquake estimated the seismic moment to be between 8.1×10^{25} dyne-cm and 2.8×10^{25} dyne-cm (Woodward Clyde Consulants, 1979). Therefore, the seismic moment obtained by modeling strong motion data is larger than that obtained by modeling long-period data for this event. Changing the fault dimensions for the Long Beach earthquake model could alter its moment without significantly affecting the fit to the strong motion data. For example, the fault surface could be made longer. Fault offset also has a direct bearing on the seismic moment of an earthquake. For example, reducing the fault offset for the preferred model of the Long Beach earthquake to, say, 50 cm results in a seismic moment of 6.2×10^{25}, the average value deduced from teleseismic data. However, this has the adverse effect of decreasing the long period response spectra for the synthetic ground motions and thus deteriorating the fit to the observed data. The influence of changing the fault offset is illustrated in Figures 2-14, 2-15 and 2-16. The short dashed curves represent the response spectra for the data and the long dashed curves and the solid curves represent the mean response spectra for a series of ground motions computed from earthquake models with fault offsets of 50 cm and 140 cm, respectively. The high frequency response spectra are not affected by changing the fault offset. In the preferred earthquake model, the slip function remains constant over the entire rupture surface. This is an idealistic representation of the rupture dynamics of a real

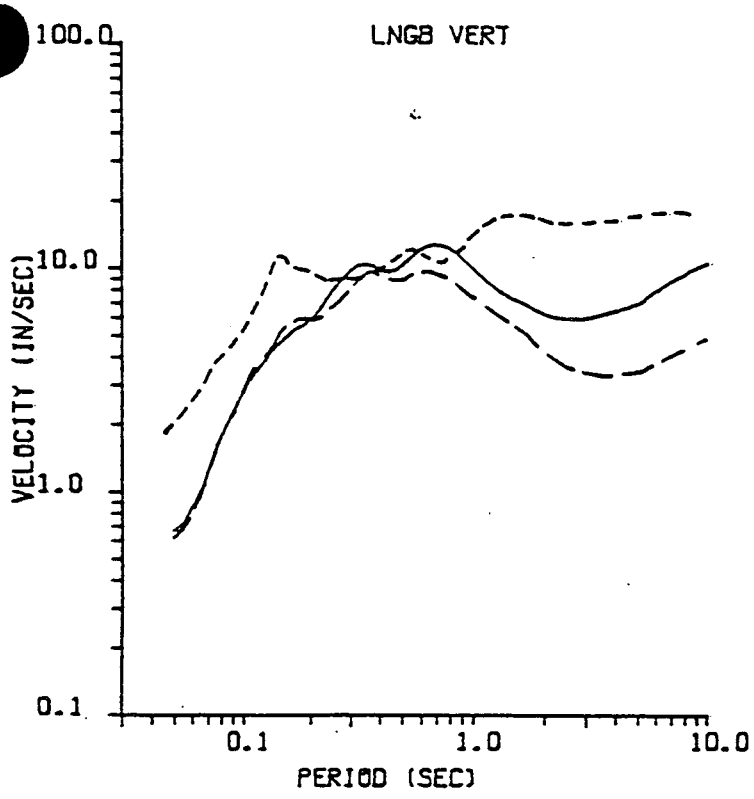

Figure 2-14. Comparison of the smoothed 2% velocity response spectra observed at station LNGB and computed from two earthquake models with different fault offsets

- - - - - - - - - Observed

——————— Calculated Mean, Fault Offset, 140 cm (Preferred Fault Model)

— — — — Calculated Mean, Fault Offset 50 cm

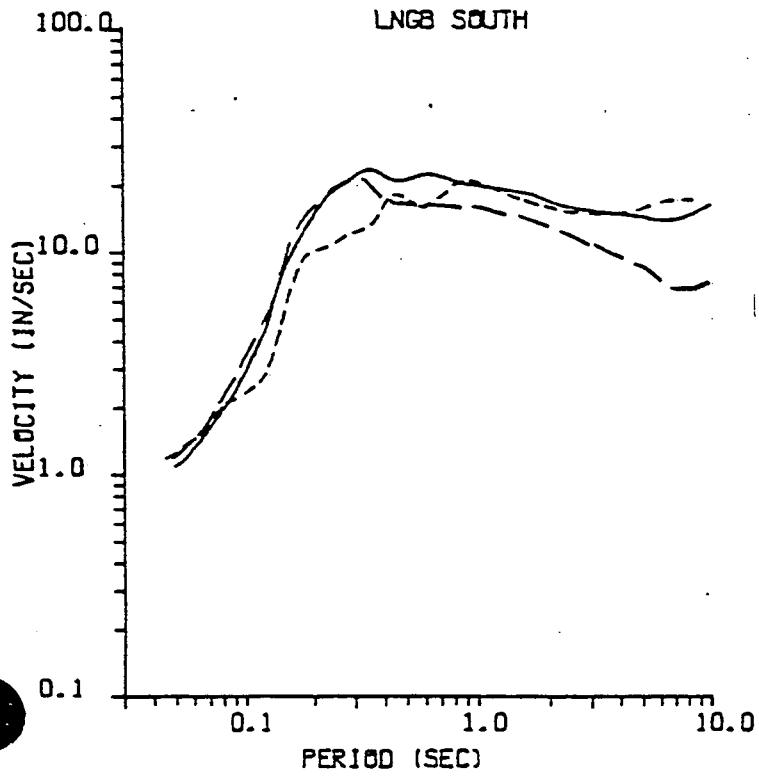

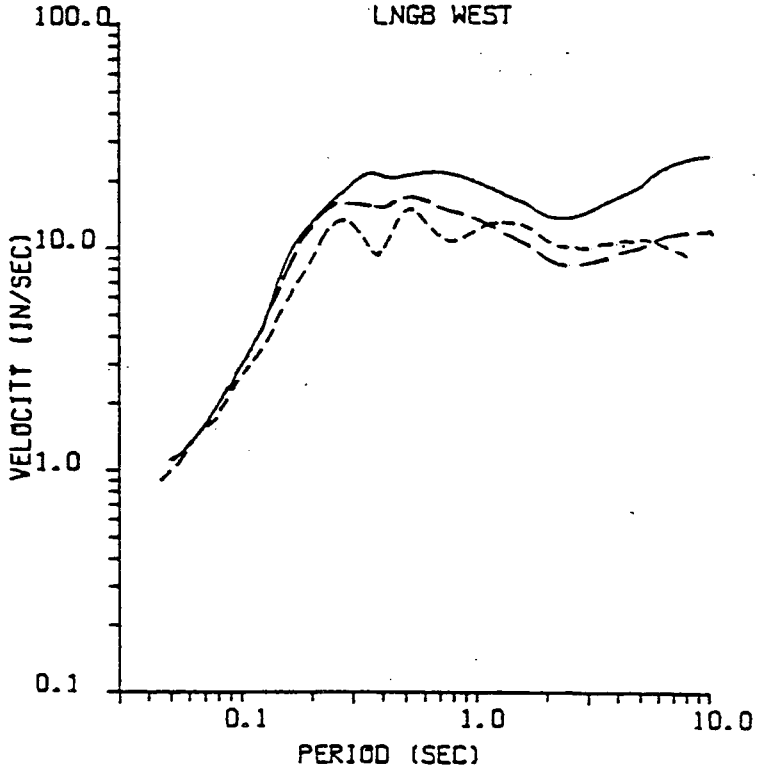

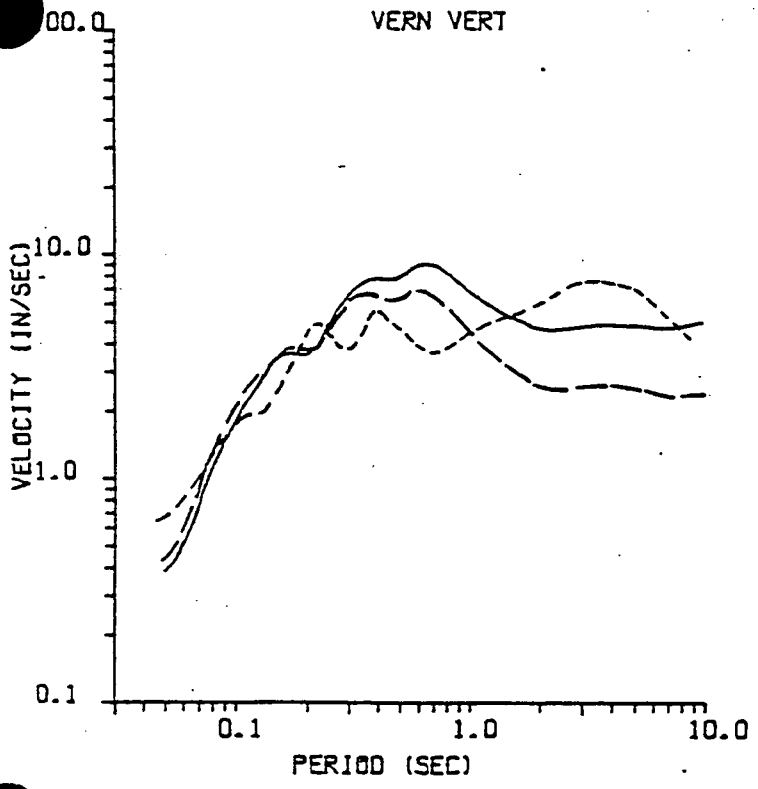

Figure 2-15. Comparison of the smoothed 2% velocity response spectra observed at station VERN and computed from two earthquake models with different fault offsets.

- Observed
- Calculated Mean, Fault Offset, 140 cm (Preferred Fault Model)
- Calculated Mean, Fault Offset 50 cm

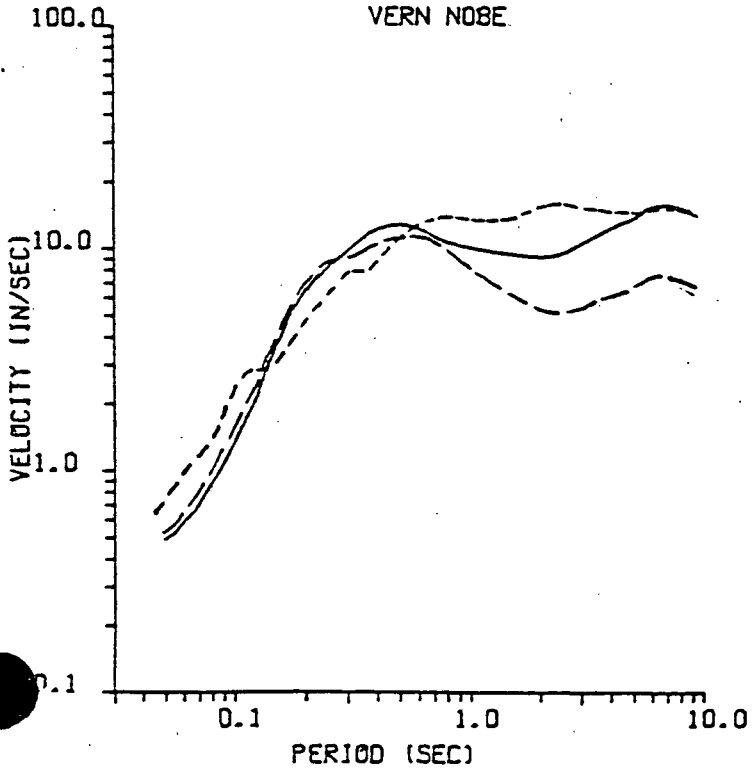

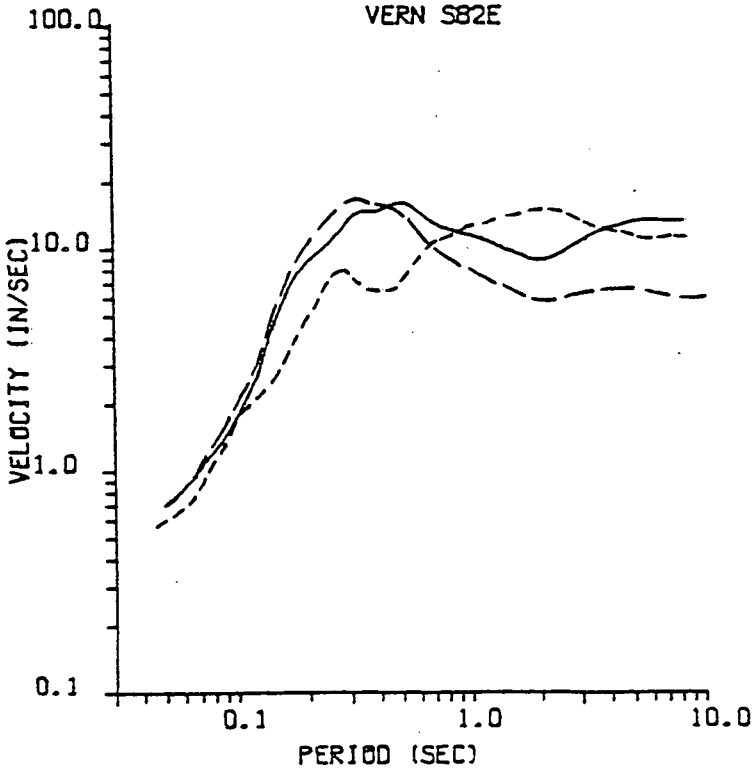

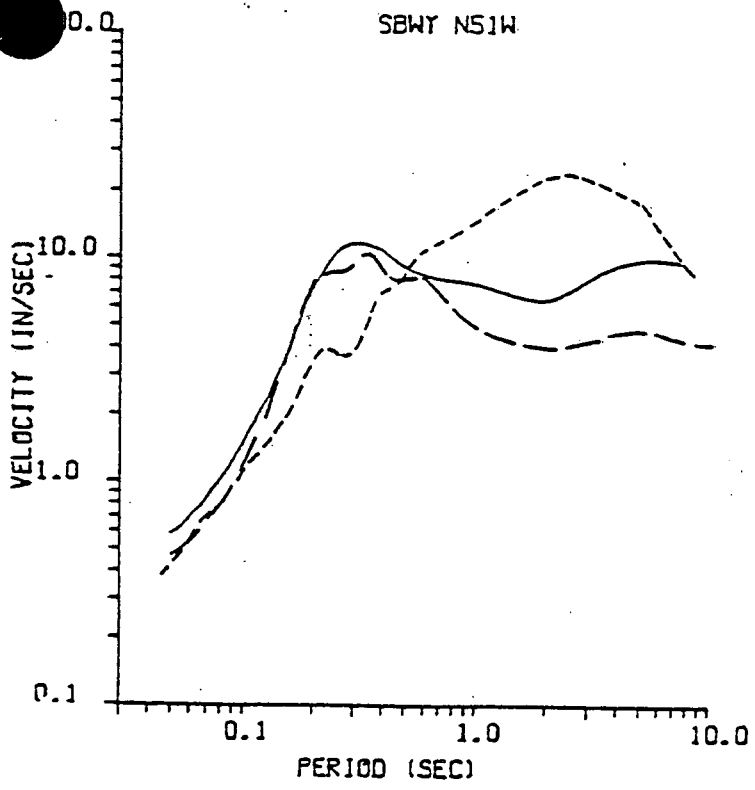

Figure 2-16 Comparison of the smoothed 2% velocity response spectra observed at station SBWY and computed from two earthquake models with different fault offsets.

Observed

Calculated Mean, Fault Offset, 140 cm (Preferred Fault Model)

Calculated Mean, Fault Offset 50 cm

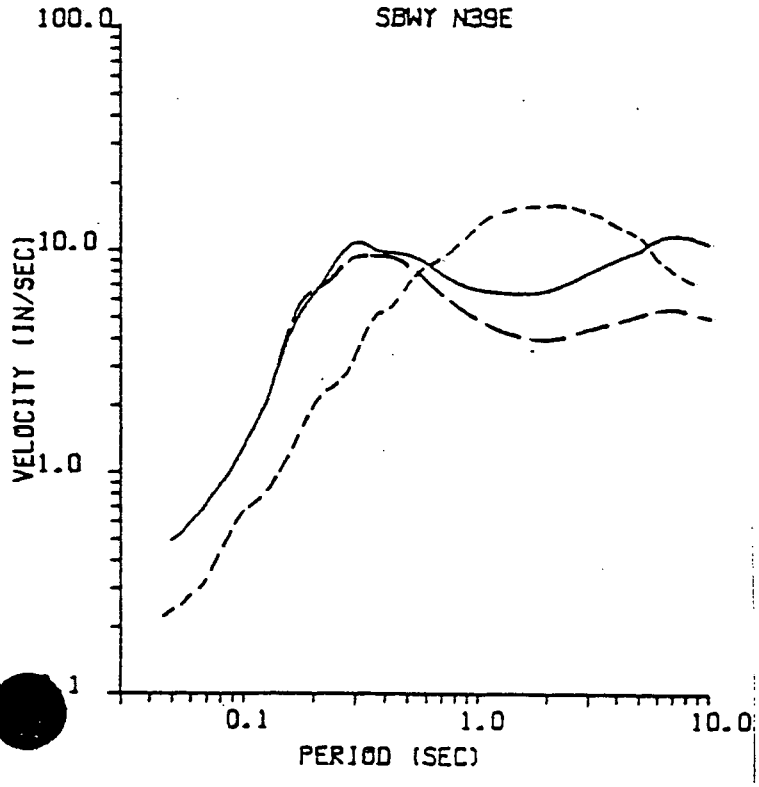

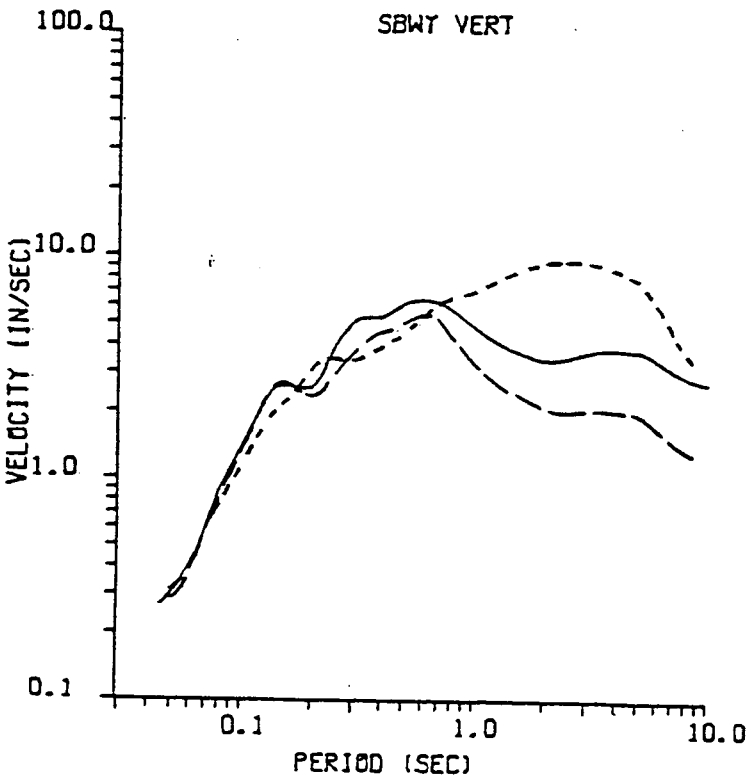

earthquake. It is not difficult to conceive of a fault offset distribution which would generate the long period spectral components observed in the recorded accelerograms, and at the same yield different values for the seismic moment. However, it is beyond the scope of this study to investigate such complicated rupture sequences. The high frequency spectral components of the recorded data can be adequately predicted using a relatively simple fault model and a constant slip function, with an initial slip velocity of 800 cm/sec.

2.4 EFFECTS OF STATION BURIAL

The ground motion recorded by a strong motion instrument can be significantly influenced when the recording instrument is situated at some depth beneath the ground surface. In this section, the effects of subsurface burial are investigated as a function of frequency for the recordings obtained at station SBWY, where the strong motion instrument was located in the train shed, 19.5 meters under Olive Street, west of the Subway Terminal Building.

A rigorous investigation into the effects of station burial at SBWY involves simulating the entire earthquake rupture using a set of Green's functions which propagate the seismic energy from each segment of rupture surface to a receiver buried at a depth of 19.5 meters, rather than to the free surface. The computational effort required to generate a completely new set of Green's functions is considerable. However, such an effort is not necessary in order to investigate the effects of subsurface burial. Instead, a representative set of Green's functions (corresponding to a representative set of rupture segments) have been calculated for a buried receiver and compared to the Green's functions calculated for the surface receiver.

The ratio of the moduli of the complex Green's function components for the buried receiver divided by the corresponding moduli for the surface receiver have been calculated at each frequency of interest, for four epicentral distances (r = 5, 20, 35 and 50 km) and three hypocentral depths (z = 2, 7 and 14 km). The ratios are nearly independent of epicentral distance and hypocentral depth, and therefore, only the results for r = 20 km and z = 7 km are presented. The ratios for the vertical, radial and azimuthal Green's function moduli are displayed in Figures 2-17, 2-18, and 2-19, respectively, as a function of frequency from 0.01 to 20 Hz. As expected, the buried receiver experiences the same ground motion as the surface receiver at low frequencies. The large peaks at higher frequency correspond to the deamplification associated with the resonance in the surface layer. For example, the fundamental mode of deconstructive interference for the azimuthal component in Figure 2-19 occurs at about

5 Hz, which corresponds to a wavelength of four times the depth of burial, h:

$$f_\beta = \frac{\beta_1}{4h} = \frac{0.4}{(4)(.0195)} \sim 5 \text{ Hz} .$$

The fundamental mode of deconstructive interference for the vertical component in Figure 2-17 is predominantly associated with compressional waves rather than shear waves and occurs at about 10 Hz:

$$f_\alpha = \frac{\alpha_1}{4h} = \frac{0.8}{(4)(.0195)} \sim 10 \text{ Hz} .$$

The higher modes of deconstructive interference occur at frequencies equal to 3, 5, 7, ... times the frequency of the fundamental mode (e.g., the second mode in the azimuthal component occurs at 15 Hz in Figure 2-19). The radial component experiences significant conversions between compressional and shear waves resulting in a more complicated behavior as a function of frequency.

By visually smoothing the resonant peaks, it may be concluded that a deamplification of approximately a factor of two occurs at frequencies higher than 2 or 3 Hz due to the subsurface burial of the instrument; there is no effect at low frequency. Such a conclusion is appropriate for an extended rupture simulation since all the Green's functions used in an earthquake modeling calculation experience similar deamplification ratios associated with the subsurface burial (and since rupture from each 1-km zone of distributed rupture is obtained by merely convolving the slip function and a trapezoidal shaped time filter with a Green's function time history -- see July 1979 report for more details).

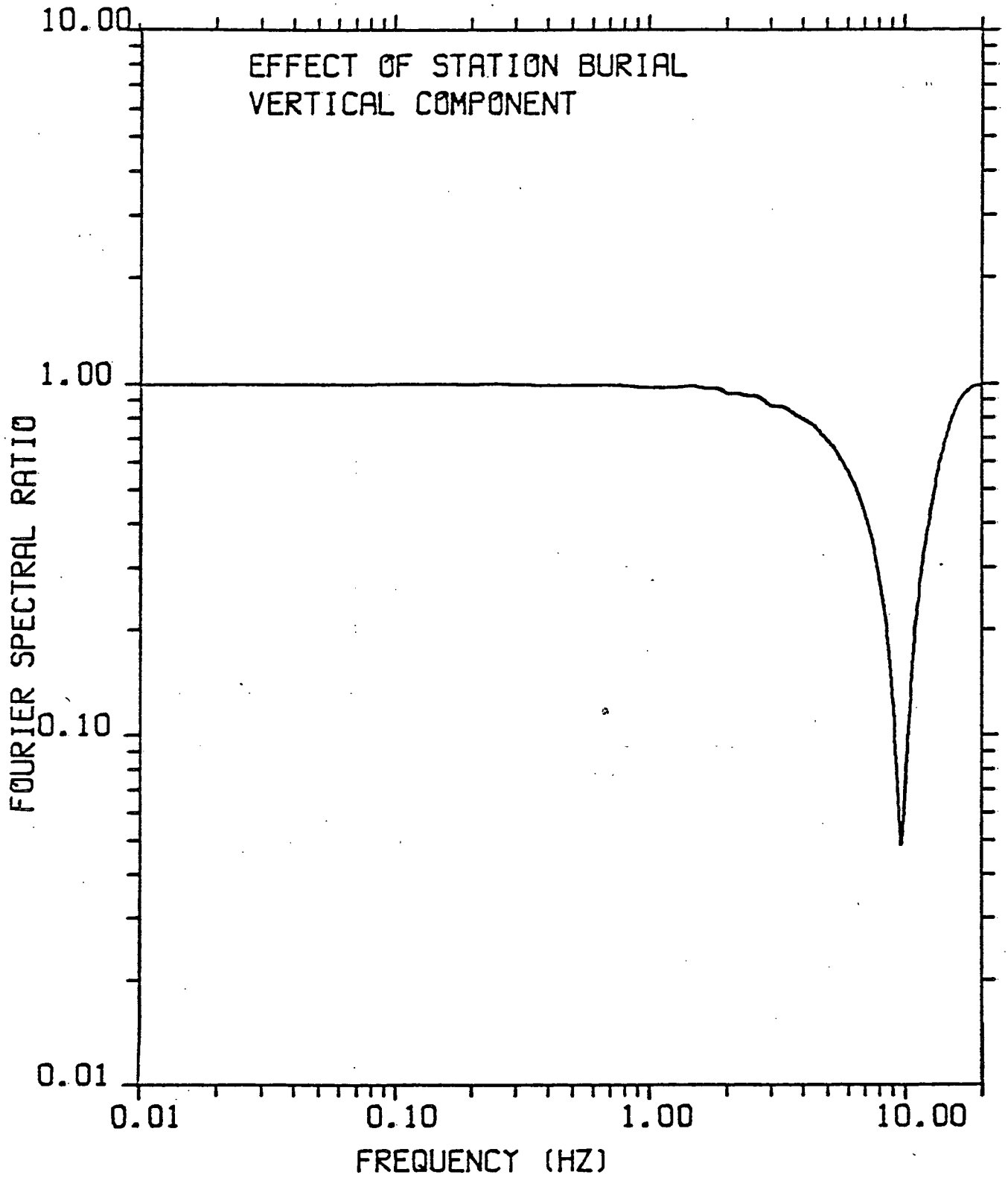

Figure 2-17. Ratio of moduli of vertical Green's function component for a receiver buried at 19.5 meters divided by the corresponding moduli for a surface receiver; results are somewhat smoothed.

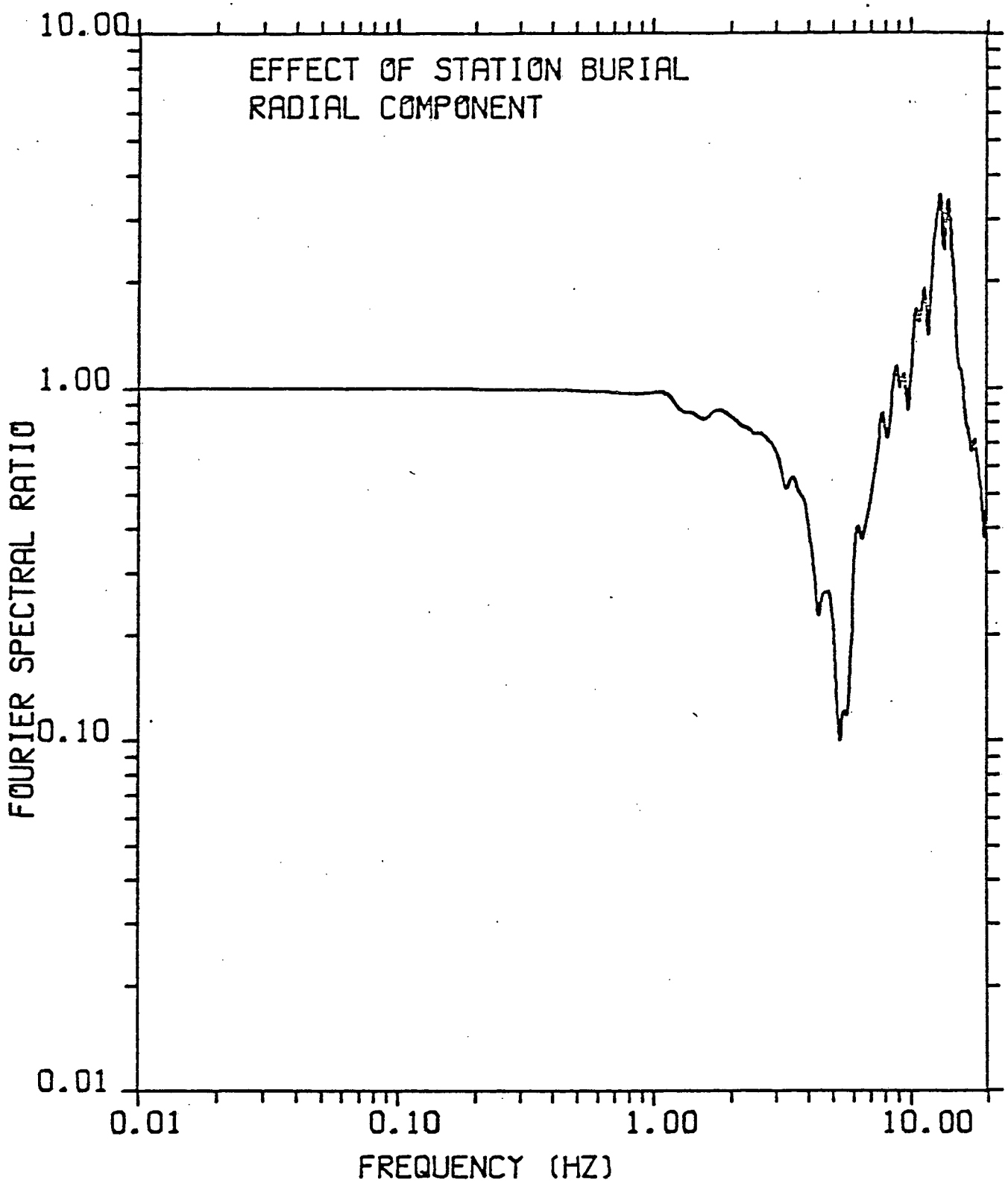

Figure 2-18. Ratio of moduli of radial Green's function component for a receiver buried at 19.5 meters divided by the corresponding moduli for a surface receiver; results are somewhat smoothed.

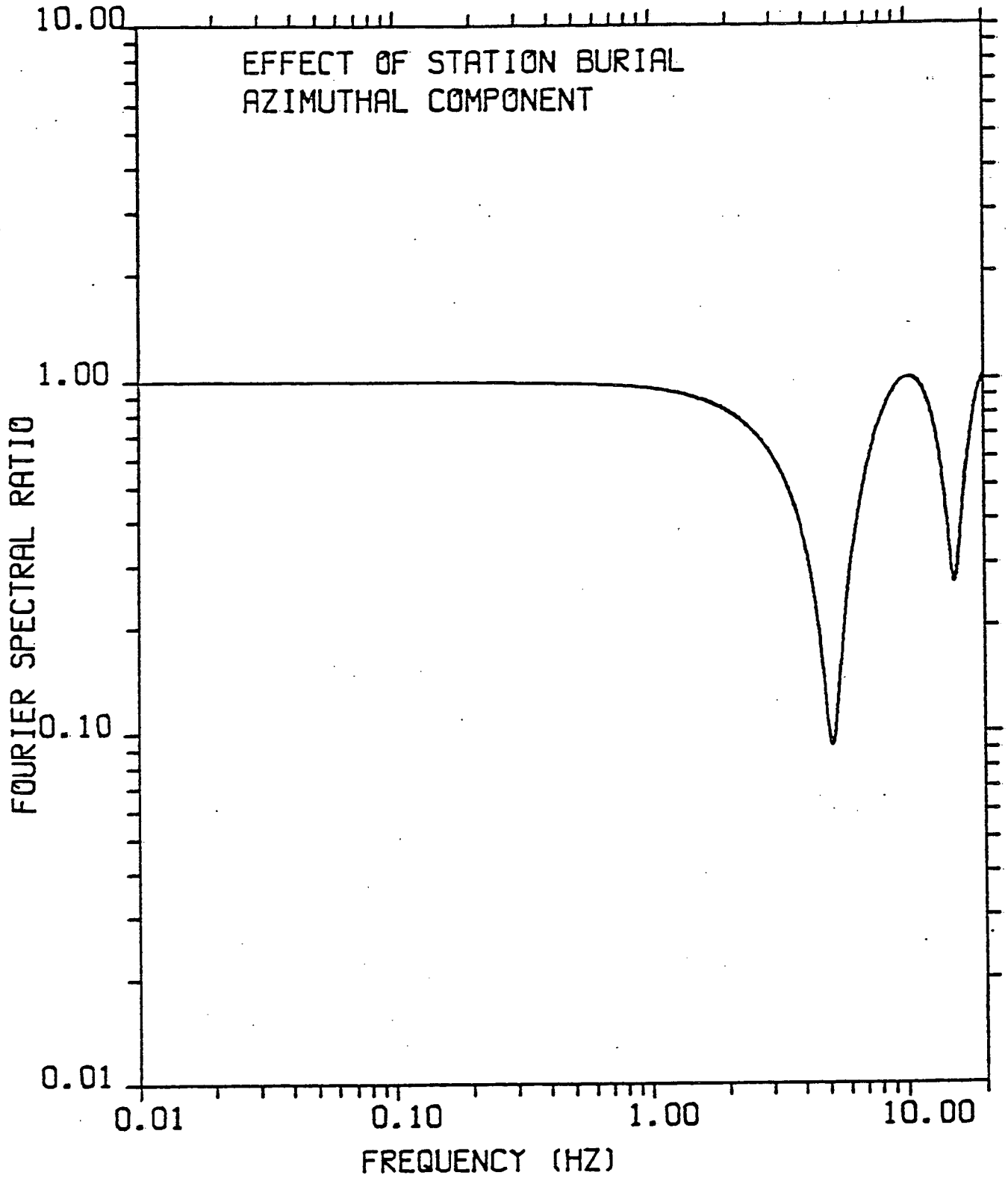

Figure 2-19. Ratio of moduli of azimuthal Green's function component for a receiver buried at 19.5 meters divided by the corresponding moduli for a surface receiver; results are somewhat smoothed.

CHAPTER 3

- MODELING THE 1971 SAN FERNANDO EARTHQUAKE

3.1 OVERVIEW AND PREVIOUS STUDIES

The 1971 San Fernando earthquake was substantially different from earthquakes likely to occur along coastal faults of California outside the regime of the Transverse Ranges. The relative block motion for the coastal faults is primarily right-lateral strike slip, characteristic of relatively low compressive stress. In contrast, the San Fernando earthquake was a predominantly dip slip (thrust) event associated with high compression. The stress drop for the San Fernando earthquake has been estimated at over 100 bars from close-in data, which is several times greater than what would be expected for a major earthquake along the coastal faults. In several respects, then, the San Fernando earthquake is a severe test of the ability for DELTA's earthquake model to simulate a large earthquake along faults in the Western United States.

Due to the proximity of the Pacoima Dam accelerograph station to the rupture surface, these strong motion recordings provide a unique opportunity to study earthquake source mechanisms. A number of researchers have derived source parameters for the San Fernando earthquake by modeling the strong motion time histories recorded at Pacoima Dam and other close-in stations. The type of time history modeled (acceleration, velocity or displacement) in each study determines the frequency range of the individual simulation techniques. A sample of the past studies includes Mikumo (1973), displacement; Boore and Zoback (1974), velocity; Trifunac (1974), displacement; Niazy (1975) acceleration, velocity, displacement; and Heaton (1978), displacement. Hanks (1974) has drawn conclusions regarding the source parameters of the 1971 San Fernando earthquake by examining the Pacoima Dam strong motion records as well as teleseismic data. Wyss and Hanks (1972), Bouchon (1978) and Langston (1978) have deduced source mechanisms for this event by modeling seismograms recorded at teleseismic distances.

Several important aspects of the faulting mechanism for the San Fernando earthquake may be deduced from the above studies. Rupture initiated several kilometers north and east of Pacoima Dam at a depth of 9 to 14 km, along a fault plane striking N60°W to N80°W and dipping 50°N to 55°N. The rupture surface is curved between the hypocenter and the surface, with the dip decreasing with decreasing depth. Directly beneath the Pacoima Dam Station, the fault plane has a dip of 20°N to 35°N. The relative block motion was predominantly thrust. The fault offset varied considerably over the rupture surface, with the largest offsets occurring near the ground surface and in the region of the hypocenter. Hence, the source mechanism for this event was quite complex relative to other Southern California earthquakes.

The single most important parameter for establishing the amplitude of high frequency ground motion during an earthquake is the initial slip velocity. A value of 800 cm/sec for the initial slip velocity has been calibrated using recordings of strike slip earthquakes in Southern California. The major objective of this study is to determine whether DELTA's earthquake model, using a constant initial slip velocity of v_o = 800 cm/sec and a relatively simple fault geometry, can match the high frequency response spectra and peak acceleration values for the strong ground motion recorded at Pacoima Dam.

The earth model used to represent the geology near Pacoima Dam consists of a viscoelastic semi-infinite half-space with the physical properties listed in Table 3-1. A half-space model was chosen because most of the faulting occurred in the crystaline basement complex of the San Gabriel Mountains. The accelerograph was situated on top of the same geologic unit.

The Pacoima Dam Station is located on a ridge in a region of large topographic gradients. Among others, Bouchon (1973), Boore (1973) and Wong and Jennings (1975) have investigated the possible effects of this type of surface topography on strong ground motion. Their results indicate that the topographic effects at Pacoima Dam may have amplified the high frequency spectral components of these recordings by as much as 50 percent.

TABLE 3-1

VISCOELASTIC PARAMETERS FOR THE SAN FERNANDO EARTH STRUCTURE

Layer Thickness (km)	P-Wave Velocity (km/sec)	S-Wave Velocity (km/sec)	ρ Density (g/cc)	Q_p Compressional Quality Factor	Q_s Shear Quality Factor
∞	5.2	3.4	2.8	243	139

The spectral components for periods greater than about one second are not affected. Since the synthetic ground motions produced by DELTA's earthquake model do not include the effects of surface topography, this so-called ridge effect has been incorporated in the comparison between calculated and observed response spectra. Figure 3-1 shows the amplification factor as a function of frequency which was used to compensate for topographic effects in the Pacoima Dam response spectra.

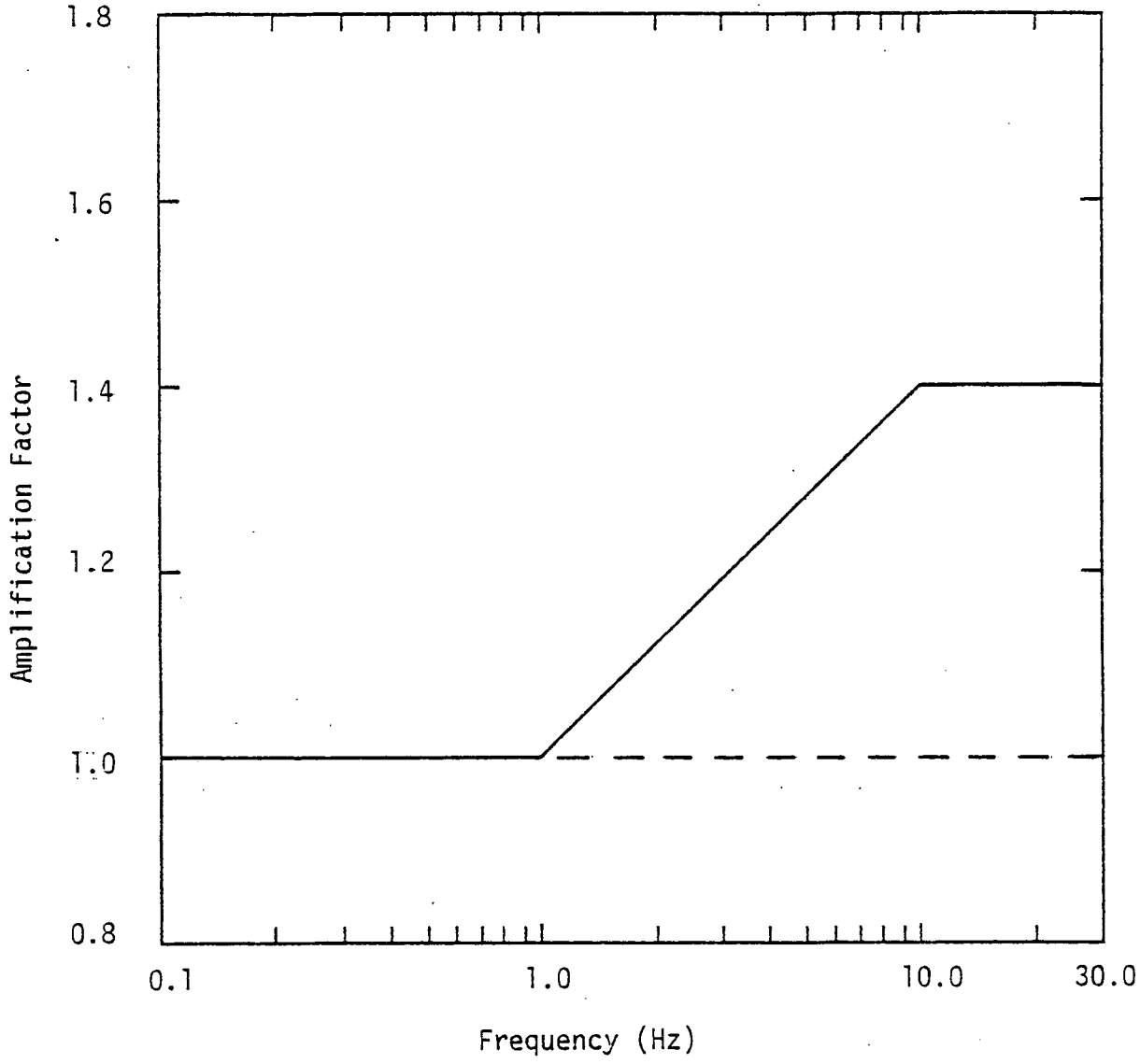

Figure 3-1. Topographic amplification factor used to compensate for ridge effect in recorded Pacoima Dam response spectra. Adapted from Figures 4 and 5, Boore (1973).

3.2 RESULTS

The fault configuration for which DELTA's earthquake model best matches the high frequency response spectra and peak acceleration values of the Pacoima Dam strong motion data is shown in Figures 3-2 and 3-3. The parameters of the preferred earthquake model are listed in Table 3-2. The San Fernando rupture surface is idealized by two fault planes which dip 24°N and 54°N and strike N75°W. The shallower fault plane intersects the free surface about 5 km southwest of the Pacoima Dam station. The hypocenter and the hinge line have depths of 11 km and 4.5 km, respectively. The initial slip velocity is constant over the entire rupture surface; v_o = 800 cm/sec. The rise times are determined by the lengths of the fault planes in the strike direction divided by the shear wave velocity. Since the slip function is constant over each fault plane, this model is simpler than those determined by matching time-domain data wiggle-for-wiggle (see, for example, Heaton (1973)).

The response spectra for the three components of computed ground motions are compared with those obtained from the observed data in Figures 3-4, 3-5 and 3-6. The solid curve in each figure represents the mean response spectra calculated from seven individual rupture simulations using DELTA's preferred earthquake model with seven independent random number sequences. The long dashed curves represent the mean response spectral values plus one standard deviation at each period. The short dashed curves show the response spectra calculated from the observed ground motion. All the curves correspond to the smoothed 2% damped response spectra. The mean and one standard deviation values for the maximum acceleration, velocity and displacement calculated using the seven independent random rupture simulations are delineated in Table 3-3 for each component of ground motion. The observed values are also shown. Taking the topographic amplification factor into account, the agreement is excellent at high frequencies.

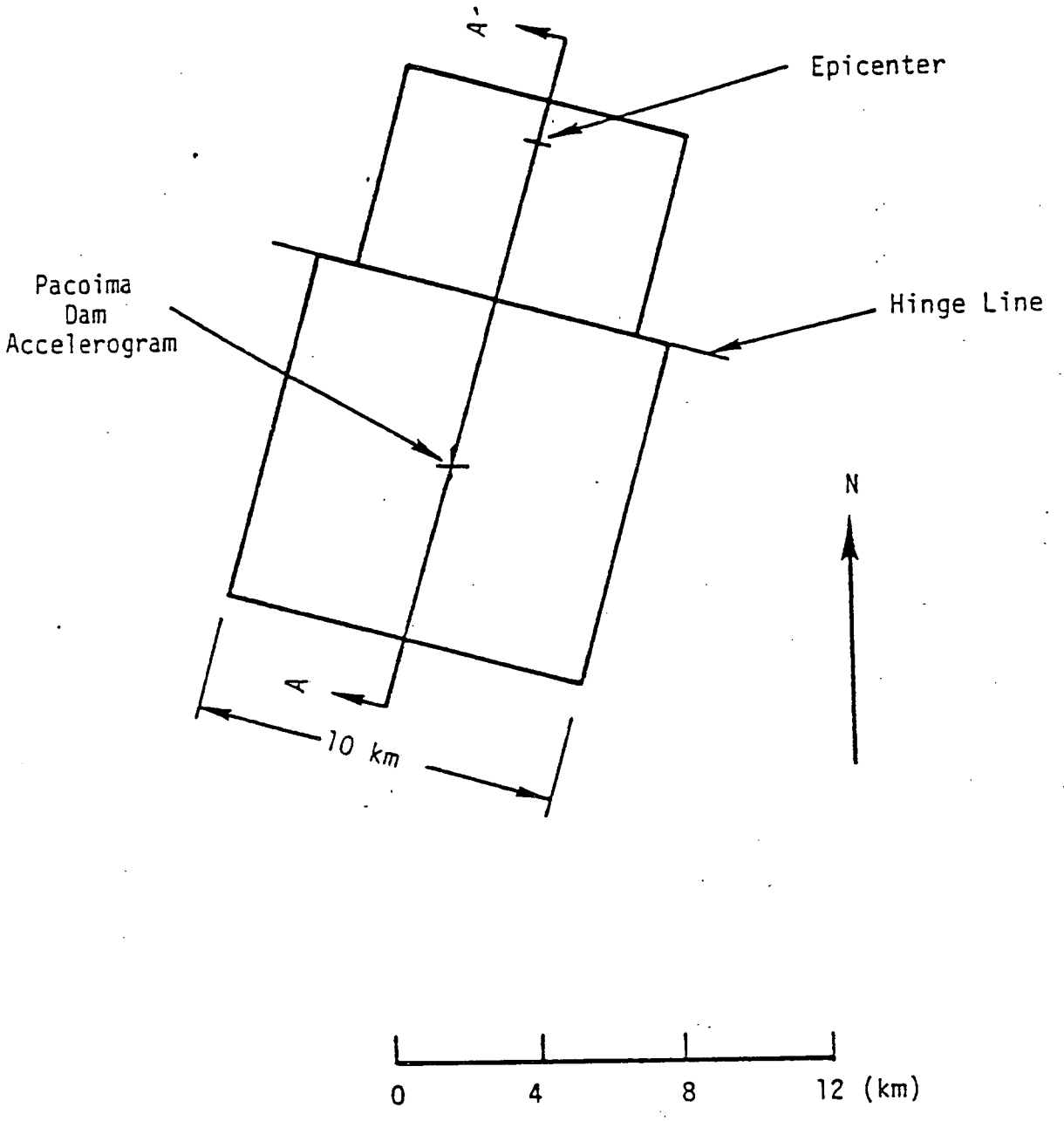

Figure 3-2. Plan view of the preferred fault model for the 1971 San Fernando earthquake.

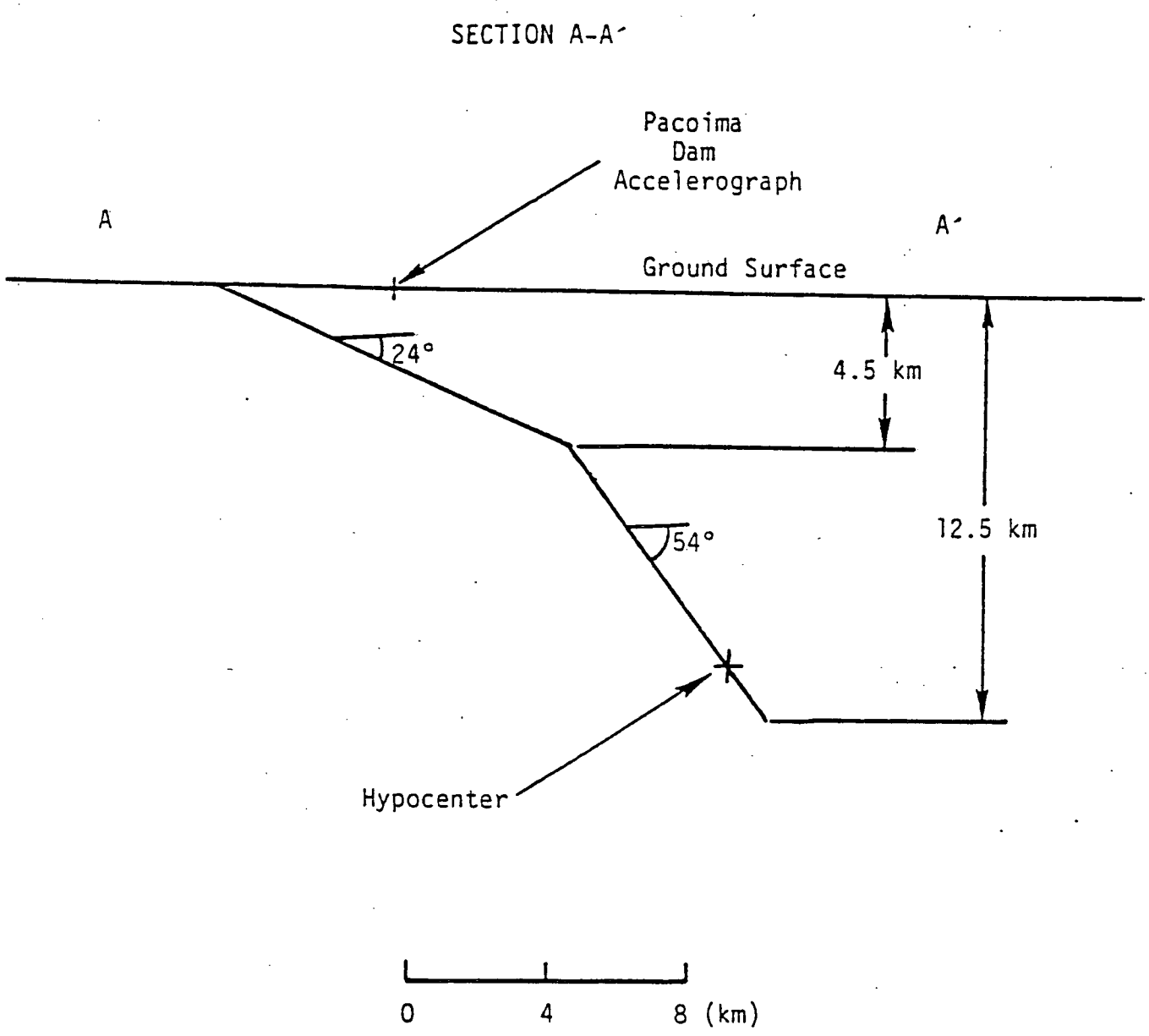

Figure 3-3. Sectional view of the preferred fault model for the 1971 San Fernando earthquake.

TABLE 3-2

PARAMETERS FOR PREFERRED MODEL OF THE SAN FERNANDO EARTHQUAKE

FAULT PARAMETERS

	Fault Length (km)	Fault Width (km)	Shallowest Extent (km)	Hypocenter Depth (km)	Strike	Dip	Slip Direction
#1	10	11	0	11.	N75°W	24°N	110*
#2	8	10	4.5	11.	N75°W	54°N	100*

SLIP FUNCTION PARAMETERS

	Initial Slip Velocity (cm/sec)	Slip Duration (sec)	Fault Offset (cm)
#1	800	2.9	350
#2	800	2.4	200

SEISMIC MOMENT

1.7×10^{26} dyne-cm

*Predominantly thrust faulting. Hanging block moves west relative to foot block.

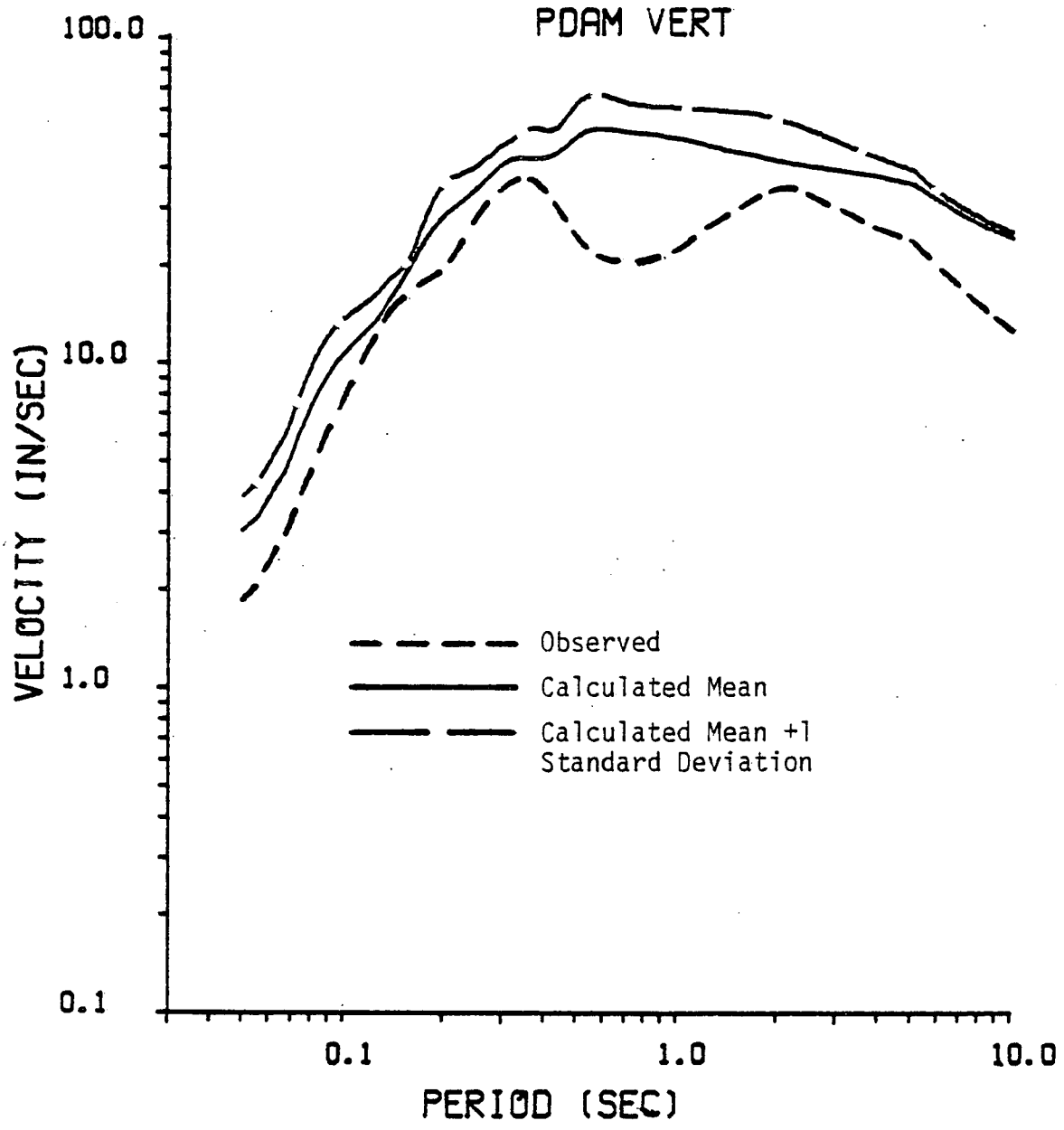

Figure 3-4. Smoothed, 2% damping response spectra for the vertical component of ground motion at Pacoima Dam. Observed data have been compensated for the ridge effect.

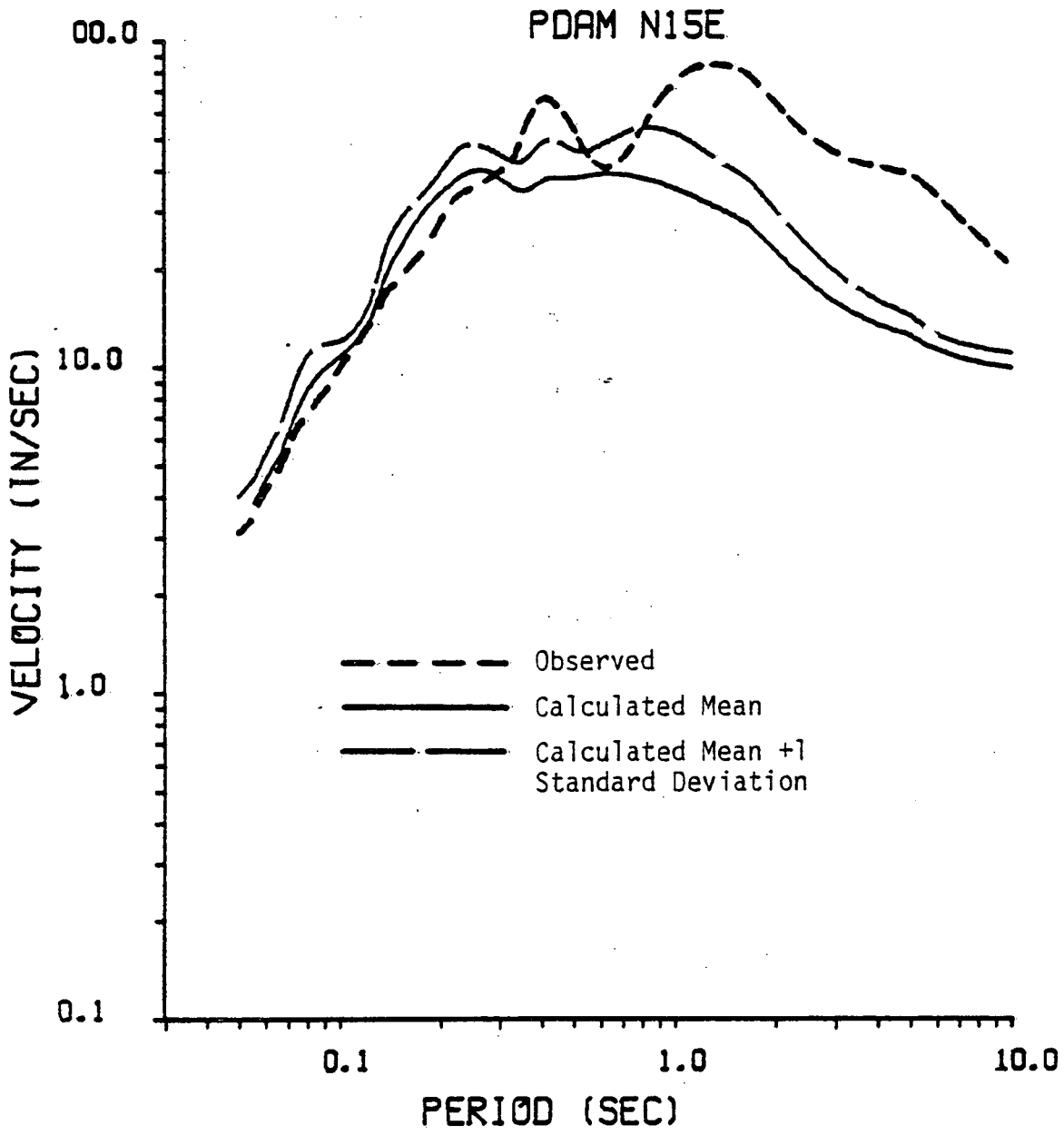

Figure 3-5. Smoothed, 2% damping response spectra for the N15E component of ground motion at Pacoima Dam. Observed data have been compensated for the ridge effect.

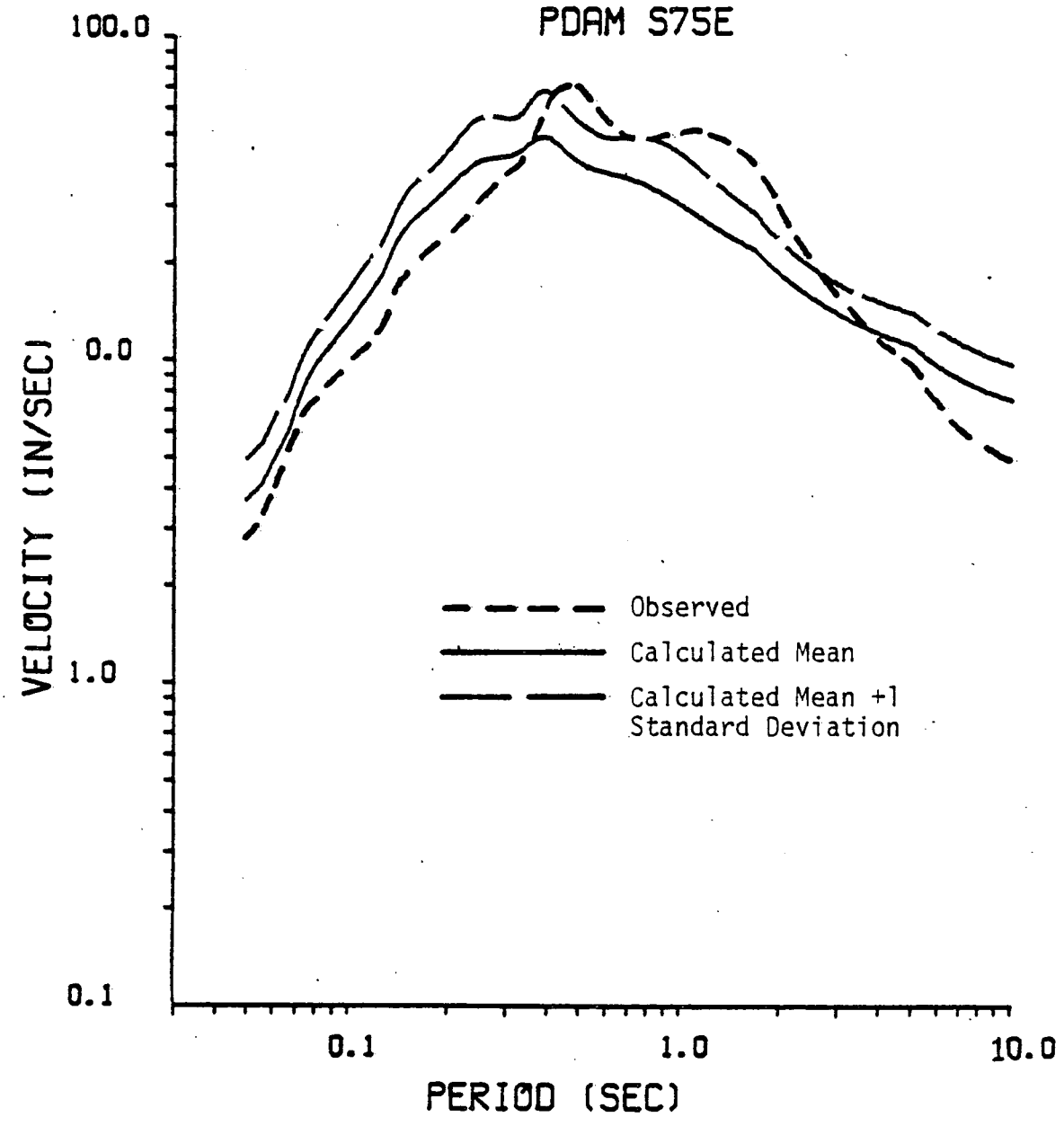

Figure 3-6. Smoothed, 2% damping response spectra for the S75E component of ground motion at Pacoima Dam. Observed data have been compensated for the ridge effect.

TABLE 3-3

MAXIMUM VALUES OF ACCELERATION, VELOCITY AND DISPLACEMENT FOR SAN FERNANDO EARTHQUAKE

Station	Component	Acceleration (g) Obs.†	Acceleration (g) Calc.*	Velocity (cm/sec) Obs.	Velocity (cm/sec) Calc.*	Displacement (cm) Obs.	Displacement (cm) Calc.*
Pacoima Dam	VERT	.71	.81 (.18)	58	110 (30)	19	49 (5)
	N15E	1.17	.84 (.03)	113	56 (15)	38	18 (4)
	S75E	1.08	.94 (.38)	58	58 (19)	11	14 (5)

*Mean values for seven simulated recordings. One standard deviation shown in brackets.

†These observations include the effect of topographic amplification which is not present in the calculated accelerations. Bouchon (1973) concludes that the ridge at Pacoima Dam amplifies the high frequency observations by 30% to 50%. Boore (1973) finds ridge amplifications as large as 50% and concludes that the free-field peak acceleration, with ridge effects removed, is 0.73 g.

At lower frequencies, the response spectra for the computed ground motion and the observed data differ somewhat, for the vertical and N15E components. This discrepancy may be attributed in part to the use of such a simplistic fault offset function. Although DELTA's earthquake modeling procedure can accomodate a spatially varying slip function, complex earthquake models of this nature are difficult to extrapolate to potential earth rupture zones.

The results of this study indicate that DELTA's earthquake model, using a constant initial slip velocity of 800 cm/sec and a relatively simple fault geometry, is appropriate for matching the high frequency response spectra for the ground motion recorded at Pacoima Dam during the 1971 San Fernando earthquake.

CHAPTER 4

CONCLUSIONS

In previous studies, DELTA's earthquake modeling capabilities were successfully used to compute strong ground motions close to major earthquake ruptures. Calibration and validation studies were carried out against the data recorded during two Southern California earthquakes: the 1940 Imperial Valley and the 1966 Parkfield earthquakes.

Further validation tests have been performed by modeling strong motion data recorded during the 1933 Long Beach and the 1971 San Fernando earthquakes. The results presented in this report indicate that the earthquake model accurately predicts the response spectral characteristics of the recorded ground motion from these important earthquakes also.

REFERENCES

Blume, J. A. (1977). Strong Motion Records of the 1933 Long Beach Earthquake, LL 44 (draft).

Boore, D. M. (1973). The Effect of Simple Topography on Seismic Waves: Implications for the Accelerations Recorded at Pacoima Dam, San Fernando Valley, California, Bull. Seism. Soc. Am., 63, pp. 1603-1609.

Boore, D. M. and M. D. Zoback (1974). Two-Dimensional Kinematic Fault Modeling of the Pacoima Dam Strong-Motion Recordings of the February 9, 1971 San Fernando Earthquake, Bull. Seism. Soc. Am., 64, pp. 555-570.

Bouchon, M. (1973). Effect of Topography on Surface Motion, Bull. Seism. Soc. Am., 63, pp. 615-632.

Bouchon, M. (1978). A Dynamic Source Model for the San Fernando Earthquake, Bull. Seism. Soc. Am., 68, pp. 1555-1576.

Del Mar Technical Associates (1978). Simulation of Earthquake Ground Motions for San Onofre Nuclear Generating Station -- Unit 1, May 1978, Final Report.

Del Mar Technical Associates (1979). Simulation of Earthquake Ground Motions for San Onofre Nuclear Generating Station -- Unit 1, Supplement 1, July 1979.

Hanks, T. C. (1974). The Faulting Mechanism of the San Fernando Earthquake, J. Geophys. Res., 79, pp. 1215-1229.

Heaton, T. H. (1978). Generalized Ray Models of Strong Ground Motion, Ph.D. Thesis, California Institute of Technology, Pasadena, California, 292 pp.

Langston, C. A. (1978). The February 9, 1971 San Fernando Earthquake: A Study of Source Finiteness in Teleseismic Body Waves, Bull. Seism. Soc. Am., 68, pp. 1-29.

Mikumo, T. (1973). Faulting Process of the San Fernando Earthquake of February 9, 1971 Inferred from Static and Dynamic Near-Field Displacements, Bull. Seism. Soc. Am., 63, pp. 249-269.

Niazi, A. (1975). An Exact Solution for a Finite, Two-Dimensional Moving Dislocation in an Elastic Half-space with Application to the San Fernando Earthquake of 1971, Bull. Seism. Soc. Am., 65, pp. 1797-1826.

Trifunac, M. D. (1974). A Three-Dimensional Dislocation Model for the San Fernando, California Earthquake of February 9, 1971, Bull. Seism. Soc. Am., 64, pp. 1393-1411.

Trifunac, M. D., and A. G. Brady (1975). On the Correlation of Seismic Intensity Scales with the Peaks of Recorded Ground Motion, Bull. Seism. Soc. Am., 65, pp. 139-162.

Wong, H. L., and P. C. Jennings (1975). Effects of Canyon Topography on Strong Ground Motion, Bull. Seism. Soc. Am., 65, pp. 1239-1257.

Woodward-Clyde Consultants (1979). Report on the Evaluation of Maximum Earthquake and Site Ground Motion Parameters Associated with the Offshore Zone of Deformation, San Onofre Nuclear Generating Station. Report Prepared for Southern California Edison by Woodward-Clyde Consultants, San Francisco, California.

Wyss, M. and T. C. Hanks (1972). The Source Parameters of the San Fernando Earthquake Inferred from Teleseismic Body Waves, Bull. Seism. Soc. Am., 62, pp. 591-602.